The neuropeptidergic connectome of *C. elegans*

Lidia Ripoll Sánchez[1,2], Jan Watteyne[3], HaoSheng Sun[4,5], Robert Fernandez[4], Seth R Taylor[6], Alexis Weinreb[7], Mark Hammarlund[7], David M Miller III[6], Oliver Hobert[4], Isabel Beets[3,†], Petra E Vértes[2,†], William R Schafer[1,3,†,#*]

1 - Neurobiology Division, MRC Laboratory of Molecular Biology, Cambridge, UK

2 - Department of Psychiatry, Cambridge University, Cambridge, UK

3 - Division of Animal Physiology and Neurobiology, KU Leuven, Leuven, Belgium

4 - Department of Biological Sciences, Howard Hughes Medical Institute, Columbia University, New York, NY, USA

5 - Department of Cell, Developmental, and Integrative Biology, University of Alabama at Birmingham, AL, USA

6 - Department of Cell and Developmental Biology, Vanderbilt University School of Medicine, Nashville, TN, USA

7 - Department of Genetics and Department of Neurobiology, Yale University School of Medicine, New Haven, CT, USA

† - Senior author

- Lead contact

***Correspondence:** wschafer@mrc-lmb.cam.ac.uk

Keywords

Neuropeptides, connectomics, networks, neuromodulation, *C. elegans*

Summary

Efforts are currently ongoing to map synaptic wiring diagrams or connectomes in order to understand the neural basis of brain function. However, chemical synapses represent only one type of functionally important neuronal connection; in particular, extrasynaptic, "wireless" signaling by neuropeptides is widespread and plays essential roles in all nervous systems. By integrating single-cell anatomical and gene expression datasets with a biochemical analysis of receptor-ligand interactions, we have generated a draft connectome of neuropeptide signaling in the *C. elegans* nervous system. This connectome is characterized by a high connection density, extended signaling cascades, autocrine foci, and a decentralized topology, with a large, highly interconnected core containing three constituent communities sharing similar patterns of input connectivity. Intriguingly, several of the most important nodes in this connectome are little-studied neurons that are specialized for peptidergic neuromodulation. We anticipate that the *C. elegans* neuropeptidergic connectome will serve as a prototype to understand basic organizational principles of neuroendocrine signaling networks.

Introduction

Understanding how behavior arises from neuronal interactions in the brain is one of the great challenges of modern neuroscience. In recent years, many projects have started to map the synaptic wiring diagrams (or synaptic connectomes) of simple and complex nervous systems to define their architecture at the cellular level[1–4]. Specifically, connectomics has aimed to identify all the individual units of the nervous system (i.e., its neurons) as well as all the connections between these units. In practice this involves reconstructing volumes of brain tissue using electron microscopy (EM), and then analyzing these images to trace neuronal processes and identify pre- and post-synaptic hallmarks of chemical synapses between identified neurons. Currently there are several endeavors of this type that are compiling complete connectomes for organisms important for neuroscience research, including *Drosophila*, *Platynereis*, *Ciona,* zebrafish, and mouse[2,3,5–7].

Although most connectomics research focuses on synaptic connectivity, chemical synapses are only one of several paths through which neurons communicate in the brain. For example, many important interactions between neurons involve volume transmission, by which secreted molecules are released extrasynaptically and activate receptors on neurons that are not wired through synapses or gap junctions to the releasing neuron. Unlike synaptic and gap junction transmission, where signaling is restricted to neurons on either side of the synapse, volume transmission can mediate signaling across distances of microns[8–10]. Such extrasynaptic signaling has been described for classical neurotransmitters as well as monoamines, and is particularly prevalent for neuropeptides, which are released from dense core vesicles outside the synaptic active zone and act on a longer temporal and spatial scale[10,11]. Although these extrasynaptic interactions are largely independent from the synaptic wiring, they play key roles in neural circuits and are thus critical for understanding the neural basis of behavior[12–18].

Neuropeptides carry out particularly complex and important functions in the brains of all organisms[19–21]. Neuropeptides are thought to be among the most ancient neuronal signaling molecules, and their origin may in fact predate the actual evolution of neurons[23,24]. Biologically-active peptides

71 are usually formed from larger genetically-encoded precursors, which are enzymatically processed
72 through proteolysis and/or chemical modification[22]. Although some neuropeptides have been shown
73 to activate ion channels or transmembrane kinases, they typically bind to G protein-coupled receptors
74 (GPCRs), which act through second messenger pathways to modulate diverse aspects of neuronal
75 physiology[25]. Neuropeptide-activated GPCRs fall into two main classes, the rhodopsin-like (Class A)
76 and secretin-like (Class B) families, and within these groups many receptors (e.g.
77 oxytocin/vasopressin, neuropeptide Y/F, neuromedin U, somatostatin) show significant conservation
78 across widely divergent animal phyla[26,27]. Neuropeptide systems also play broadly conserved roles in
79 the control of behavioral states, including those involved in feeding, sleep and arousal, reproductive
80 behavior, and learning[14,28–33]. In humans, the role of neuropeptides as neuromodulators has made this
81 signaling system a highly sought-after target for new neuropsychiatric treatments. Currently 50 drugs
82 acting via GPCRs have been approved by the FDA[34], including several neuropeptide-GPCRs such as:
83 orexin antagonists for treatment of insomnia[35], a substance P antagonist for treatment of
84 chemotherapy-induced nausea[36]. Besides new treatments are being developed like a GIP agonist as
85 treatment for Alzheimer and Parkinson's[37]. These promising therapies and the large number of
86 remaining neuropeptide-GPCRs in humans[18,38] indicate the therapeutic potential of this molecular
87 system.

88 The diversity and extent of neuropeptide signaling implies that the pathways for peptidergic
89 communication can also be considered as a network. The genomes of all animals encode many, in
90 some cases hundreds of neuropeptides, along with a similarly large number of GPCRs[18,39–41].
91 Moreover, in contrast to monoamines, which are typically expressed in only a small subset of neurons
92 in the brain, neuropeptides are expressed extremely broadly; indeed, recent single-cell transcriptomic
93 studies indicate that most if not all neurons in the mouse cerebral cortex express one or more
94 neuropeptides as well as multiple neuropeptide-binding GPCRs[39,42]. These data imply that peptidergic
95 signaling underpins a dense and pervasive interaction network involving most if not all neurons of an
96 animal's nervous system[43,44]. Since neuropeptide signaling is thought to be mostly extrasynaptic, the
97 topology and structure of this wireless neuropeptide connectome is expected to be fundamentally

98 distinct from that of the wired synaptic connectome[45]. However, in most organisms there is
99 insufficient gene expression data mapped with single-cell resolution to identified neurons to map the
100 structure of these extrasynaptic networks.

101 The nematode *C. elegans* represents an attractive animal to investigate the structure and
102 organization of neuropeptide signaling networks due to its small and well-characterized nervous
103 system. *C. elegans* was the first and is currently still the only adult organism with a completely
104 mapped synaptic neuronal connectome, with each of its 302 neurons and approximately 2300 synaptic
105 connections identified through electron microscopy (EM) reconstructions[46–48]. Despite its small size,
106 the *C. elegans* nervous system has been found to share several structural features with that of larger
107 animals. For example, the *C. elegans* connectome, like those of larger nervous systems, exhibits a
108 small-world topology, with relatively high clustering paired with relatively short average path
109 lengths[49,50]. Likewise, the *C. elegans* nervous system is highly modular, with functionally segregated
110 local clusters of high within-group connectivity[51–54]. Finally, the worm connectome contains a small
111 number of highly connected hubs, which are interconnected in a core or rich club and facilitate
112 communication between modules[55]; similar rich club topology has been observed in bigger brains,
113 including the human cortex[56,57]. Shared structural features are also apparent at the microcircuit level;
114 for example, feed-forward motifs are significantly overrepresented in the nematode connectome, just
115 as in the mammalian cortex[58–60]. Thus, insights gained from analysis of neuropeptide signaling
116 networks in *C. elegans* may also reveal organizational principles that are conserved in larger brains.

117 Although the *C. elegans* nervous system is anatomically small, at the biochemical level its
118 neuropeptide signaling pathways show similar complexity and remarkable conservation with humans
119 and other larger-brained animals. Its genome contains 159 predicted neuropeptide precursor genes
120 (NPP) (including 40 insulin-like peptides) that produce over 300 different neuropeptides[22,61].
121 Likewise, approximately 150 *C. elegans* genes encode GPCRs known or predicted to be activated by
122 neuropeptides[25,62]. These numbers are of a similar order of magnitude to the numbers of neuropeptides
123 and peptide activated GPCRs in the human genome[18,63]. Each *C. elegans* neuron not only expresses at

124 least one neuropeptide and at least one neuropeptide receptor, as do vertebrate neurons,[18,39,40,42,43] but
125 each *C. elegans* neuron class expresses a unique combination of neuropeptide-encoding genes[40], a
126 notion that illustrates the tremendous potential complexity of neuropeptide signaling. Many *C.*
127 *elegans* neuropeptides and cognate receptors are phylogenetically conserved across animal phyla and
128 have clear human homologues, with some families (such as the RFamide peptides) having undergone
129 expansion in the nematode lineage[64]. Thus, neuropeptide signaling in nematodes shows surprising
130 conservation as well as similar diversity to neuropeptide signaling in the human brain, despite vast
131 differences in neuron number and anatomical complexity.

132 Here we present a draft connectome of neuropeptidergic signaling in *C. elegans,* built by
133 integrating gene expression, ligand-receptor interaction, and anatomical datasets. We identified
134 predicted neuron-to-neuron signaling interactions mediated by 91 neuropeptide-receptor pairs, and by
135 aggregating these individual neuropeptide-signaling networks generated a comprehensive network of
136 peptidergic signaling in the *C. elegans* nervous system. This resulting neuropeptidergic connectome
137 differs significantly in its structure from the previously-characterized wired connectome[47]; for example,
138 it is denser, contains distinct hubs, high-weight edges, and autocrine signaling foci, and has a
139 decentralized topology allowing direct communication among a large fraction of neurons. We expect
140 this nematode neuropeptide connectome will serve as a prototype for understanding the organization of
141 peptidergic signaling and how it interacts with the wired neural circuitry in other organisms, including
142 those with much larger brains.

143 **Results**

144

145 **Construction of a neuropeptidergic connectome**

146 To generate a draft neuropeptide connectome, we integrated information from three datasets to infer
147 potential pathways for neuropeptide signaling between individual *C. elegans* neurons (Figure 1A). To
148 identify biologically relevant molecular interactions between individual neuropeptides and receptors,
149 we used data from a large-scale reverse pharmacology screen which tested 55,386 potential

150 neuropeptide-receptor interactions *in vitro* and identified 461 peptide-GPCR couples encoded by 55
151 neuropeptide and 57 GPCR genes[40]. To determine which neurons express each neuropeptide and
152 receptor, we used publicly available single-neuron transcriptome data from the CeNGEN project, which
153 described single-cell RNA-sequencing transcription profiles of all predicted neuropeptide and peptide-
154 activated GPCR genes in *C. elegans*[40]. We validated these scRNA datasets with several CRISPR/Cas9-
155 engineered reporter alleles of ligands and receptors. Finally, we used previously published EM
156 anatomical reconstructions to assess physical constraints on potential diffusion of neuropeptides to their
157 target receptors[48,65,66]. In constructing the neuropeptide network, we consider that two neurons (nodes)
158 are connected by a directed edge if the first neuron expresses a particular neuropeptide ligand and the
159 second expresses a paired receptor, subject to spatial constraints on signaling (Figure 1B).

160 For each dataset, it was necessary to threshold for biologically relevant interactions.
161 For biochemical interactions, the raw dataset contained 461 neuropeptide-receptor pairs that showed
162 dose-dependent activation with a half-maximal effective concentration (EC_{50}) ranging between 0.1 pM
163 to 22 μM[64]. At the gene level, these pairs were encoded by 55 neuropeptide and 56 GPCR genes, with
164 148 unique gene-gene interactions. In assessing neuropeptide-receptor pairings we initially opted for a
165 conservative EC_{50} threshold of 500 nM, as many neuropeptide-receptor couples with EC_{50} values in this
166 range have been validated *in vivo*[14,25,28,32,62]. By this criterion, we defined 91 individual neuropeptide-
167 receptor gene couples, with a large number (51) of the predicted neuropeptide GPCRs having at least
168 one identified ligand. The ligand-receptor interactions were complex, with several peptides activating
169 more than one receptor (promiscuous receptors) and several receptors being activated by multiple
170 peptides encoded by distinct precursor genes (versatile peptides)[64].

171 We next sought to determine an appropriate threshold for the scRNA-based gene expression
172 dataset. The transcriptomic data from the CeNGEN project has been differentially thresholded based
173 on a ground-truth dataset of reliable gene expression from across the whole *C. elegans* nervous
174 system using fosmid or receptor tagged reporters[40]. Each threshold was given a false discovery rate
175 and a true positive rate depending on the number of correctly identified cells for a given gene by the
176 scRNAseq analysis[40]. To determine the most appropriate threshold for our analysis, we obtained
177 single-copy genomic knock-in reporters for 17 representative neuropeptide precursor genes and 9

representative genes for neuropeptide receptors and characterized their expression patterns comprehensively using the NeuroPAL marker strain (Figure 2A, B). For both we found that threshold 4, although on some occasions overly stringent, was a good approximation of the expression pattern (Figure 2; Supplemental Table 1-3). Thus, although this stringent threshold has lower discovery power and thus may undercount the number of neurons expressing each gene, its stringency minimizes the likelihood that our resulting network will contain edges that do not represent authentic paths for potential neuropeptide signaling.

Evaluating spatial constraints on neuropeptide signaling

These biochemical and gene expression datasets allowed us to infer which neurons express neuropeptide and receptor genes that could mediate a neuromodulatory interaction; however, the physics of diffusion and the neuroanatomy of the animal might potentially constrain some of these interactions *in vivo*. We therefore considered several possible models of the neuropeptidergic network based on different anatomical and spatial constraints (Figure 3B, C). We used EM reconstruction data for each individual neuron in the *C. elegans* nervous system to identify its anatomical location (Figure 3A, Supplementary Table 4) and the neuropil bundles into which their axons and dendrites project[48,65,66]. In the first and most permissive model, long-range signaling is permitted and neuropeptidergic connections can take place between any neurons in the system. In the second ("mid-range") model, neuropeptidergic connections can occur only between neuronal processes in the same anatomical area, such as the head (including pharynx), tail and midbody (Figure 3A). In the third ("short-range") model, we only considered potential peptidergic connections between neurons in the same neuronal process bundle, that is, between neurons whose processes overlap in the nerve ring, ventral or dorsal cord, or an auxiliary nerve. Finally, it has recently been shown that the nerve ring, into which more than half the neurons (168) project, can be divided into four layers or strata based on patterns of physical contact[67,68]. We therefore also considered a fourth model in which neuropeptide signaling inside the nerve ring is constrained within individual strata and thus between neurons that make physical contact.

205 To evaluate each model, we investigated whether the expression patterns of receptors and
206 ligands were consistent with neuropeptide signaling being restricted as described above (Figure 3B,
207 C). For example, if neuropeptide signaling occurred only between neurons in physical contact (as in
208 model 4) we would expect neurons expressing a given receptor to project to the same nerve ring strata
209 as neurons expressing its ligand. To simplify this analysis, we focused on the neuropeptide-receptor
210 couples in which the receptor has only one ligand and the neuropeptide only binds to that receptor,
211 assessing whether, under the constraints of each model, there would be receptor-expressing neurons
212 that were unable to receive a signal from any neurons expressing its ligand. Conversely, we also
213 analyzed couples where the ligand activated only one receptor, asking whether under a given model
214 there were ligand-expressing neurons that could not communicate with cells expressing its receptor.
215 This analysis appeared to argue against the most restrictive model, in which ligands could not
216 diffuse between nerve ring strata. Specifically, we observed many examples in which a neuropeptide
217 receptor was expressed only in strata that did not express its specific ligand (Figure 3B, C, orange
218 points). For instance, while the *capa-1* neuropeptide precursor gene is expressed only in the ASG
219 sensory neuron, which projects its axon into the fourth nerve ring stratum, the gene for its receptor
220 NMUR-1 is expressed in all four strata[32,69](Figure 3B, C). Thus, NMUR-1 receptors in strata 1-3 must
221 be activated by CAPA-1 peptides that diffuse from their release site in stratum 4. Overall, 37 of the 41
222 receptors analyzed were expressed in at least one neuron making no contact with a neuron expressing
223 its ligand. Likewise, 32 of the neuropeptide precursor genes were expressed in at least one neuron
224 making no contact with neurons expressing its receptor (Figure 3C, yellow points). Since the nerve
225 ring strata are not separated by glial or other barriers, and experimental evidence[14,32] indicates
226 neuropeptides can indeed travel between strata, it is reasonable to infer that neuropeptides are not
227 likely to be constrained by anatomical layers in the nerve ring or other neuronal bundles.
228 We likewise observed cases in which the expression of a neuropeptide or receptor gene
229 implies mid-range signaling between distinct nerve bundles in the same body region (Figure 3B, C).
230 For example, the *frpr-7* receptor gene is expressed in multiple pharyngeal neurons, while its ligand
231 FLP-1 is released exclusively from the AVK neuron whose processes lie in the nerve ring and ventral
232 cord[13]. Thus, FRPR-7 receptors in the pharynx must be activated by peptides released by AVK in the

233 nerve ring, consistent with published evidence that neuropeptides can signal between head neurons
234 and pharyngeal neurons[13,70]. Indeed, for a majority (14/22) of the receptors expressed in pharyngeal
235 neurons, their ligand was expressed only outside the pharynx (Figure 3B, red points). Likewise,
236 receptors such as NPR-3 and TRHR-1 are expressed in the CAN neurons, yet their ligands FLP-15
237 and NLP-54 respectively are not expressed in any neurons projecting into the canal-associated nerve[71]
238 (Figure 3B, C, CAN neurons labelled). Thus, we hypothesize that at least some neuropeptide
239 signaling occurs between different nerve bundles, in particular between the pharynx and the nerve
240 ring and between CAN and other nerves in the body. We therefore focused our subsequent analysis on
241 model 2, consisting only of stringently selected short-range interactions, and model 3, which includes
242 mid-range signaling between nerve bundles in the same body region.
243
244 **Neuropeptide networks exhibit diverse topologies**
245 Based on these criteria, we first constructed network graphs between neuropeptide-expressing
246 and receptor-expressing neurons for each of the 91 individual neuropeptide/receptor couples in our
247 dataset (Supplementary Figure 1, 2). These networks were filtered by removing edges between
248 neurons that did not project an axon or dendrite into the same process bundle (for the short-range
249 network) or into the same body region (for the mid-range network). In their short-range version, 78 of
250 these ligand-receptor couples formed a single connected network, whereas 13 formed networks with
251 two or even three disconnected components (Figure 4B, Supplementary Figure 1). In their mid-range
252 versions, all 91 couples formed a single connected network (Supplementary Figure 2).
253 We observed a diverse range of topologies in the networks for individual peptide-receptor
254 couples. One topological measure in which the different networks varied was their assortativity, or the
255 extent to which nodes are preferentially connected to nodes of similar degree. Using the conservative
256 short-range model, we observed that most of the networks, including many of those highly conserved
257 in evolution, were local networks, in which both ligand and receptor were expressed in relatively
258 restricted sets of neurons (Figure 4A, Supplementary Figure 1). The neurons in these networks
259 showed relatively low average degree and often encompassed only a subregion of the total nervous
260 system. In addition, we found 8 highly disassortative *integrative* networks, with many low-degree

261 peptide-releasing neurons signaling to relatively few high-degree receptor-expressing neurons (Figure
262 4A). We also observed 23 disassortative *broadcasting* networks that are characterized by a small
263 number of high-degree peptide-releasing neurons that signal to many low-degree receiving neurons
264 with broadly expressed receptors (Figure 4A, Supplementary Figure 1). Interestingly, both integrative
265 and broadcasting networks involved promiscuous receptors with multiple ligands, specifically FRPR-
266 8, EGL-6, DMSR-7, and DMSR-1. DMSR-7 and DMSR-1 also figured prominently in a fourth
267 category of more assortative, pervasive networks, in which both the ligand and receptor show broad
268 expression and most neurons thus show relatively high degree (Figure 4A, B). Relaxing the spatial
269 restrictions on our model had relatively modest impact on network topology, with four networks that
270 are local in the short-range model becoming either integrative (one network) or broadcasting (3
271 networks) in the mid-range model (Supplementary Figure 2). Thus, the topologies of neuropeptide
272 networks appear relatively robust to our assumptions about the spatial scope of neuropeptidergic
273 signaling.

274 **The neuropeptide connectome is a decentralized, dense network**

275 By aggregating the networks from the individual neuropeptide-receptor couples, we next
276 compiled complete neuropeptide connectome networks based on short-range or mid-range signaling
277 (Figure 5). Even for the more conservative short-range network, in which signaling was restricted to
278 neurons with processes overlapping in the same bundle, the density of connections was remarkably
279 high, with more than a third of all possible connections or edges (0.3437) present in the network.
280 Allowing mid-range connections (0.4429) or long-range connections (0.5929) increased this density
281 further (Supplementary Figure 3A, B). By comparison, the *C. elegans* synaptic (0.0251) and
282 monoamine (0.0236) networks were far less dense, fourteen-fold lower than the short-range
283 neuropeptide network. We also computed edge weights for the connections in the neuropeptide
284 networks based to the number of neuropeptide-receptor pairs capable of signaling between two nodes.
285 We observed that a large number (35% in the short-range network) of neuron pairs were connected by
286 only a single neuropeptide-receptor interaction, but some (9%) were connected by 6 or more different
287 peptide-receptor couples (Figure 5). In the most extreme case, we observed that two neurons, the
288 AVD premotor interneurons and the PQR oxygen-sensing neurons, were linked by 18 different

289 neuropeptide-receptor pairs, suggesting extraordinarily complex patterns of signaling could exist
290 between these cells (Figure 5, highlighted). Interestingly many other high-weight, biochemically
291 complex connections occurred between neurons of the oxygen sensing circuit and were mediated by a
292 common set of promiscuous receptors (DMSR-1, DMSR-7 and FRPR-8) and versatile neuropeptides
293 (FLP-4, FLP-9, FLP-10 and FLP-13). These neurons are thus connected by multiple neuropeptidergic
294 channels of communication, potentially allowing complex regulation by context and experience.
295 A striking feature of the midrange network in particular was its integration of neurons
296 disconnected from the synaptic connectome. For example, the 14 neuron classes of the pharyngeal
297 nervous system form a heavily synaptically interconnected, functionally autonomous network akin to
298 vertebrate enteric nervous systems, which is topologically isolated from the rest of the nervous
299 system[65,72,73]. We find that unlike the wired connectome, there are no neuropeptidergic networks that
300 define circuitry exclusively in the pharynx; to the contrary, pharyngeal neurons are fully integrated
301 into the somatic nervous system via strong reciprocal interconnectivity (Figure 5). All pharyngeal
302 neuron classes receive 90% or more of their incoming connections from outside the pharynx. Some
303 classes of pharyngeal neurons also broadcast extensively to the somatic nervous system, with several
304 (I1, I3, I4, I5, M5 and NSM) having more than 100 outgoing connections (more than 90% of their
305 total) to non-pharyngeal neurons. Likewise, it is notable that the CAN neurons, which completely lack
306 chemical synapses, show strong and reciprocal neuropeptidergic connectivity with the rest of the
307 nervous system, indicating that this unusual neuron class is well embedded in the neural network
308 (Figure 5, CAN highlighted).
309 We next investigated topological features of the aggregate neuropeptide network. In
310 particular, we analyzed the degree nodes of the network, defined as the number of incoming (in-
311 degree) and outgoing (out-degree) connections made by each neuronal node. Degree is often an
312 indicator of functional significance in networks, since high-degree nodes or hubs often play key
313 functional roles in the brain and other complex systems. As expected from the high density of
314 neuropeptide signaling, the average degree of both the short-range (Figure 6A) and mid-range
315 networks (Figure 6B) were significantly higher than for the previously characterized synaptic (Figure
316 6C) and monoamine (Figure 6D) networks. Moreover, when we analyzed the distribution of degree

317 across the neuropeptide networks, we observed relatively flat curves with many high-degree nodes;
318 more than half the neurons in the short-range network and nearly two thirds in the mid-range network
319 had a degree higher than 200, indicating that they have in and out connections with more than a third
320 of all other neurons (Figure 6A, B). In contrast, the synaptic network was much more centralized,
321 with only 10 neurons having degree greater than 50 (Figure 6C); similarly, the monoamine network
322 had only 18 high (>50) degree neurons (Figure 6D). The best-connected neurons in the neuropeptide
323 network have exceptionally high in-degree as well as out-degree, indicating that their status as hubs
324 depends as much on incoming connections as outgoing connections, and as much on their expression
325 of broadly-signaling neuropeptides as on integrating GPCRs (Figure 6A, B); this contrasts with the
326 monoamine network, where the hubs are exclusively monoamine-releasing neurons with a high out-
327 degree (Figure 6D).
328
329 **The neuropeptide connectome contains a highly connected core with unique peptidergic hubs**
330 A significant feature of many networks is the so-called rich club property. In such networks,
331 the most highly connected hubs form more connections between themselves than expected based on
332 their high degree alone; these hubs therefore comprise a rich club or core of the network that
333 facilitates communication between more peripheral network nodes. The *C. elegans* synaptic
334 connectome, for example, contains a rich club consisting of 11 premotor interneurons that appear to
335 play important roles in driving global brain states[55,74]. Remarkably, we found that the neuropeptide
336 connectome also shows the rich club property, but its rich club consists of 156 neurons (166 in mid-
337 range network), more than half of the nervous system (Figure 6F). Within the rich club the density of
338 connections is 0.6834 ($p<0.00001$), more than double the density of the overall network (0.3427).
339 Interestingly, compared to the wired synaptic connectome, the neuropeptide connectome as a whole
340 has significantly higher clustering and reciprocity (i.e. neurons are more likely to connect in both
341 directions) but lower modularity and disassortativity. This finding further supports the notion of a
342 decentralized neuropeptide connectome, with a broad-based densely-connected core allowing direct
343 communication between a large fraction of neuron pairs.

344 To further investigate the relationship between neuropeptide and synaptic signaling, we
345 looked at the correlation between synaptic and neuropeptidergic degree (Figure 6G). We observed
346 that neuropeptide degree and synaptic degree were positively correlated ($p < 0.0001$, $r = 0.53$). We
347 further observed that neurons with a high synaptic degree were among the most important
348 neuropeptidergic hubs; for example, all 11 members of the synaptic rich club (DVA, PVCL/R,
349 AVAL/R, AVBL/R, AVDL/R, AVEL/R) were among the 25 highest-degree nodes in the short-range
350 neuropeptide network (Figure 6G). However, there were also several neurons of very high degree in
351 the neuropeptide connectome but unexceptional synaptic degree (Figure 6G); these neurons can be
352 described as specialized for neuropeptide signaling. Six neurons (AVKL/R, PVQL/R, PVT and PVR)
353 had higher short-range neuropeptide degree than any of the synaptic rich club neurons (Figure 6A); if
354 mid-range signaling is considered these same six neurons remain the highest-degree hubs (Figure 6B).
355 Interestingly, the AVKL/R and PVT neurons are notable for expressing no classical neurotransmitters
356 or monoamines[75], while the PVQL/R neurons appear anatomically specialized for neuropeptide
357 signaling due to a preponderance of dense core vesicles[14,76]. AVKL/R, and PVT have been previously
358 linked to the control of global behavioral states related to sleep and arousal[14,73], but the functions of
359 the other neuropeptide hub neurons PVQ and PVR are not well-characterized.
360
361 **The neuropeptide connectome core has a defined mesoscale structure**
362 To further probe the structure of the neuropeptide connectome we investigated whether the
363 network contained modules or other forms of mesoscale substructure. We first applied standard
364 methods for modular decomposition, but the high density of the network precluded the identification
365 of any discrete modules, unless we aggressively filtered out lower-weight edges where neurons were
366 connected only by a small number of neuropeptide-receptor interactions. However, we hypothesized
367 that other types of meso-scale structure may be present[52,77]. We wondered for example whether we
368 could identify subgroups of neurons with similar patterns of incoming and outgoing neuropeptide
369 connections. We therefore applied dimensionality reduction methods (Principal Component Analysis
370 (PCA) and t-SNE) to the connectivity matrix of the aggregate neuropeptide networks to identify
371 groups of neurons that share a connectivity pattern. This analysis highlighted 3 clearly defined groups

372 of neurons that receive similar incoming connections, along with a more diffuse cloud of neurons with
373 more variable connectivity (Figure 7A, B). Interestingly the three clusters comprise most neurons of
374 the neuropeptidergic network (155 of 302), 76% of which are also members of the neuropeptidergic
375 rich club (112; Figure 7A, B). Interestingly, each group receives a characteristic range of incoming
376 connections, and this alone is enough to significantly sort them into these groups ($p<0.0001$) (Figure
377 7D): group 1 neurons have indegree of 134-156 (mean rank 162.2), group 2 neurons have an indegree
378 of 252-282 (mean rank 276.5), group 3 neurons have an indegree of 169-212 (mean rank 222.9), and
379 neurons in the unclustered cloud have an indegree below 169 (mean rank 77) (Figure 7D).
380 These groups also diverge in the neuron types that form them and to which they are connected
381 (Figure 7C, E). Group 1 is mostly motorneurons (motor core), including those involved in locomotion
382 (VA, DA, VB, and DB)[78] and the grouping of these neurons is driven by inputs from the posterior
383 touch mechanosensory neurons PVM and PLML/R[79] and the interneuron PVWL/R (Figure 7C).
384 Group 2 neurons are a mix of interneurons and motorneurons, including all top neuropeptidergic hubs
385 (hubs core), that receive connections from every other neuron type, with the neuropeptidergic hubs
386 (PQR, PVT and PVR) particularly important drivers for the grouping (Figure 7C). Finally, group 3
387 neurons are a mix of pharyngeal neurons, interneurons, motorneurons and sensory neurons (sensory
388 core) that receive connections from every other neuron type but motorneurons, with RIR and
389 pharyngeal neurons I5 and I4 driving the cluster (Figure 7C). Interestingly, although the characteristic
390 neural inputs of the groups differed substantially, the most important (highest indegree) neuropeptide-
391 receptor interactions for each group, involved versatile neuropeptides FLP-9, FLP-11 and FLP-16 and
392 promiscuous receptors DMSR-7 and DMSR-1 (Figure 7C), leading to interconnections between
393 groups (Figure 7E). For example, Group 1 forms connections with itself, Group 2 and with the
394 unclustered cloud but not with Group 3; Group 3 forms connections with Group 2 and unclustered
395 cloud neurons but not Group 1, and Group 2 forms connections with all other groups. Thus, Group 2
396 serves as a link with Groups 1 and 3, which have few direct connections with each other.
397
398 **Co-expression of neuropeptides with their target receptors generates autocrine pathways**

399 Signaling cascades, in which a neuropeptide receptor is specifically co-expressed with a non-
400 cognate peptide whose release it controls, are a classic hallmark of neuroendocrine pathways. To
401 investigate whether the *C. elegans* neuropeptide connectome contains such cascades, we evaluated co-
402 expression between neuropeptide and receptor genes. We performed a Fisher's test to look for
403 neuropeptide genes and GPCR genes that are co-expressed in the *C. elegans* nervous system more
404 often than expected from their individual expression frequencies. We identified 121 peptide-receptor
405 pairs meeting this criterion (Supplementary Figure 4A), only 5% of which corresponded to cognate
406 neuropeptide-receptor pairs (autocrine connections). Using these peptide-receptor pairs as nodes and
407 the neuropeptide-receptor interaction data to form edges between them, we built a network of
408 overrepresented signaling cascades within the larger neuropeptide connectome (Supplementary Figure
409 4B). This network is fully connected and provides a simplified view of how neuropeptide signaling
410 pathways interact within the nervous system.

411 Co-expression of a neuropeptide receptor with its own ligand will generate a self-loop or
412 autocrine connection, in which release of the peptide can signal back onto the sending cell. If we
413 consider all cases where a peptide and its receptor are co-expressed in a given neuron, we find that 58%
414 of the *C. elegans* nervous system harbors putative autocrine peptide connections (Figure 8A and 8B).
415 Autocrine signals appear most prevalent in neurons categorized as either interneuron or motorneuron
416 (Figure 8B), although two of the three types with the largest number of autocrine connections (URX
417 and PQR) are sensory neurons. Promiscuous receptors participate more in autocrine peptide signaling
418 (Figure 8C, Suppl. Figure 8D), the most prominent of which are DMSR-1 and DMSR-7 (Figure 8C).
419 We observed a strong positive correlation between the number of different autocrine peptide
420 connections that a neuron harbors to its degree within the neuropeptide network (Figure 8D, left panel),
421 with some but not all neuropeptide hubs showing a high diversity of autocrine signaling. In contrast,
422 weak to no correlations were observed between autocrine connection diversity and the synaptic, gap
423 junction, or monoamine connectomes.

424 Autocrine connections were especially prevalent in specific circuits in the *C. elegans* nervous
425 system. For example, both URX and PQR, which have among the highest diversity of autocrine
426 signaling, are key sensory neurons that mediate *C. elegans'* responses to aversive O_2 levels[80–82]; other

427 O_2 sensory neurons (AQR and BAG) also co-express ligand-receptor pairs, though to a lesser degree
428 (Figure 8E, bottom left). As O_2 sensing neurons tonically signal ambient O_2 concentrations[83], autocrine
429 signaling may play a stabilizing role in maintaining the homeostasis of neuronal activity. Autocrine
430 neuropeptide signals are also prevalent in the neuromuscular circuit of the ventral nerve cord (VNC –
431 Figure 8F, bottom right) which mediates locomotion[84]. These autocrine loops are primarily mediated
432 by eight RFamide-related neuropeptides that activate two promiscuous receptors, DMSR-1 and DMSR-
433 7, although other receptors such as NPR-5 are also involved (Supplementary Figure 5F). Interestingly,
434 autocrine signaling is restricted to the excitatory A- and B-class VNC motorneurons which drive
435 backward and forward locomotion, respectively[84]; in contrast, both D-type inhibitory motor neurons
436 and the excitatory AS motorneurons, which play modulatory roles in both forward and backward
437 crawling[85], do not co-express any neuropeptide-GPCR pairs. It should be noted that some autocrine
438 peptidergic pathways are shared between neighboring excitatory motorneurons in the VNC, raising the
439 possibility that they might coordinate activity and/or neurosecretion across excitatory motorneurons in
440 a paracrine manner[86–89]. Heterogeneity in autocrine neuropeptide pathways within the A- and B-class
441 motorneurons (Supplementary Figure 5F) hints at heterogeneity in the contribution of individual
442 motorneurons in this process.
443
444 **Discussion**
445 **Neuropeptide signaling forms a complex wireless network**
446 Neuropeptide signaling has long been recognized as critical to brain function, yet despite
447 recent advances in connectomics, the structures of neuropeptidergic signaling networks are largely
448 uncharacterized. We have generated a draft neuropeptide connectome by integrating information from
449 three datasets: a biochemical deorphanization screen matching neuropeptidergic GPCRs with their
450 ligands, a scRNAseq dataset characterizing the expression patterns of all peptide and receptor genes at
451 the single neuron level, and an anatomical dataset defining the morphologies and neuron-neuron
452 contacts of all *C. elegans* neurons. The resulting connectome is remarkably dense; even a short-range
453 network with the most conservative assumptions about the spatial diffusion of neuropeptides was

454 more than ten-fold denser than the previously mapped synaptic connectome of *C. elegans*. As we have
455 also used conservative assumptions regarding gene expression thresholds and ligand-receptor
456 affinities, and since approximately half the putative neuropeptide-activated GPCRs remain to be
457 deorphanized, the actual neuropeptide connectome is almost certainly even more dense than the draft
458 network described here. However, based on sensitivity analysis it seems clear that the overall
459 structure and topological features of the neuropeptide connectivity are likely to hold even when more
460 connections are added to the network (Supplementary Figure 3A-B).

461 A particularly salient feature of the neuropeptide connectome is its decentralized topology,
462 which contrasts sharply with the more centralized structure of wired neural connectomes. Synaptic
463 connectomes from worms to humans are characterized by a core of high-degree hubs, which are
464 interconnected to form a rich club. This rich club, which in *C. elegans* consists of 11 premotor
465 interneurons, occupies a central position in the connectome, connecting local modules and
466 coordinating their activity. Rich clubs have been previously linked to important functional properties;
467 for example, in *C. elegans* the synaptic rich club has been shown to be involved in global brain states
468 related to locomotion[55,74], and in *Drosophila melanogaster* the synaptic rich club constitutes the
469 sensorimotor integrative center of the organism[90]. The gap junction and monoamine connectomes of
470 *C. elegans* likewise contain relatively small rich clubs of less than 20 neurons of relatively high
471 degree. In contrast, the neuropeptide connectome contains a rich club of (in the short-range network)
472 156 neurons, more than half the neurons in the entire nervous system. The neurons in this
473 neuropeptidergic rich club are extremely well-connected to each other as well as to the rest of the
474 nervous system; all have a degree greater than 203 (in the mid-range network degree of 251), meaning
475 they both send and receive direct connections from at least 40% of all neurons. This remarkable
476 decentralization may be a feature of neuropeptide signaling networks in other organisms[43,44,91].

477 **Implications of neuropeptide network structure for neuronal computation**

478 The decentralized structure of the neuropeptidergic connectome implies that the strategies it
479 uses for computation and information flow may differ significantly from those employed by the more
480 centrally-organized synaptic network. Intriguingly, both nematode and mammalian neuronal types
481 appear to express nearly unique combinations of neuropeptides and receptors, serving as a molecular

482 bar code for neural identity[40,43]. Thus, the source of a signal may be encoded by the precise
483 combination of peptides released by the sending neuron. The dynamics of neuropeptide release are
484 also likely to be critical to the information conveyed by peptidergic signals. For example, acute
485 release of FLP-20 peptides by mechanosensory neurons has been shown to trigger short-term sensory
486 locomotor arousal in response to touch stimulation, while chronic release of FLP-20 peptides from the
487 same neurons mediates long-term cross-modal plasticity in olfactory circuits when the sense of touch
488 is lost[14]. Future studies of such mechanisms are likely to provide general insights into how
489 neuropeptide networks encode information in the brain.

490 Despite its highly dense connectivity, the core of the neuropeptide connectome exhibited a
491 clear substructure. When input patterns were analyzed using dimensionality reduction methods, the
492 neurons in the network core could be divided into three clear groups, one containing mainly
493 pharyngeal and sensory neurons, a second containing the highest degree interneurons, and a third
494 containing many motorneurons. These three groups are themselves connected in a defined pattern,
495 with the second group linking the first and third groups which show few direct links with each other.
496 This organization contrasts in interesting ways with the organization of many synaptic networks, in
497 which peripheral neurons form modules with high internal connectivity that connect to each other
498 through the hubs of the rich club core. In the neuropeptide connectome the core itself exhibits a clear
499 meso-scale organization, forming 3 distinct groups of neurons defined not by unusually high intra-
500 group connectivity, but by intra-group similarity of incoming and outgoing connections patterns. This
501 is in line with recent work showing the existence of different types of meso-scale organization[77] and is
502 also reminiscent of stochastic block modelling approaches previously applied to the *C. elegans*
503 synaptic connectome[52]. It will be interesting to see if neuromodulatory and synaptic networks from
504 other nervous systems show a similar diversity on meso-scale structure. We expect that looking
505 beyond classical modules is likely to become increasingly important as we begin to look at cellular-
506 scale connectomes of larger organisms, with classes of sensory neurons that are not interconnected but
507 have similar connectivity profiles and perform similar functions.

508 **Identification of neuropeptide signaling hubs**

509 Although the rich club of the neuropeptide connectome is extensive and encompasses a large
510 portion of the *C. elegans* nervous system, some neurons within this group are of particularly high
511 degree and therefore may play key roles in neuromodulatory signaling. Perhaps not surprisingly, the
512 premotor neurons of the synaptic rich club are also highly connected in the neuropeptide connectome;
513 all 11 of these neurons show a neuropeptide degree above 400 in the short-range network. Since these
514 neurons are known to play important roles in driving global brain states[14,74,76] it is logical that they
515 would also be important targets of neuromodulatory control. In addition, the neuropeptide
516 connectome contains 6 neurons whose neuropeptide degree is higher than any of the synaptic rich
517 club (degree > 490). Three of these neurons (PVT and the pair of AVK neurons) are specialized
518 peptidergic neurons that express no classical neurotransmitter or monoamine and have been linked to
519 arousal and sleep-like behaviors[14,92,93]. Specialized neuropeptidergic neurons have also been
520 described in other organisms, and in mice they have been linked to global behaviors such as fear[94].
521 The other peptidergic hubs (PVR and the pair of PVQ neurons) are tail neurons that extend long
522 processes to the nerve ring, and in the case of the PVQs (as well as PVT) these processes are rich in
523 dense-core vesicles[48,65,66]. Since AVK also has a long process (extended from its cell body in the head
524 through the nerve ring and the ventral cord to the tail) these neurons may be morphologically
525 specialized for local release of peptides throughout the nervous system. While AVK is known to play
526 roles in arousal and motor control, the functions of the remaining neuropeptide hubs (or of other
527 neurons of high neuropeptidergic degree such as PVN and PVP) are largely uncharacterized. Given
528 their importance in the neuropeptide signaling network, it will be interesting in the future to explore
529 the roles of these neurons in the control of behavioral states.
530 It is interesting to note that even in the long-range network, where no spatial restrictions on
531 neuropeptide diffusion are imposed, the six short and mid-range hub neurons retain their central
532 importance in the network. This confirms that the high degree of the hubs in the short- and mid-range
533 networks is not merely an artifact of the spatial conditions we imposed but rather is a consequence of
534 expressing key combinations of neuropeptides and receptors. Notably, the long-range network
535 contains additional high-degree nodes that are not hubs in the short- and mid-range networks, in
536 particular the oxygen-sensing neurons URX, AQR, PQR and BDU and the tail motorneurons DA09

537 and VA12. One might speculate that these neurons could in fact engage in long-range neuroendocrine
538 signaling, and that the long-process morphology of the short- and mid-range hubs might allow them to
539 carry out neuropeptide modulation on a finer temporal or spatial scale. In the future, these questions
540 may be addressable using *in vivo* probes for neuropeptide receptor signaling[95,96].

541 **Neuropeptide signaling links specific components of the nervous system**

542 In addition to these high degree nodes, the neuropeptide connectome also contains edges of
543 unusually high weight, representing neuron pairs linked by multiple neuropeptide-signaling pathways.
544 While many neuron pairs in the network are connected by a single neuropeptide pathway, 17 pairs of
545 neurons are linked by 15 or more different neuropeptide-receptor couples. Most of these extremely
546 high-weight edges involve connections between the oxygen-sensing neurons PQR or URXL/R and the
547 motor circuit (either the DB motorneurons or the AVD premotor interneurons). Why might oxygen-
548 sensing neurons participate in so many complex neuromodulatory interactions? These neurons
549 strongly influence locomotor states and their tonic responses to ambient oxygen are influenced by
550 experience and other sensory cues. Complex neuropeptide signaling may allow feedback between the
551 oxygen sensors and motorneurons to fine-tune the activity of this circuit across time and space.

552 The oxygen-sensing neurons and the motor circuit were also found to be important sites for
553 autocrine signaling, in which a neuropeptide receptor and its ligand are co-expressed in the same
554 neuron. Autocrine peptide signaling is ubiquitous in other brains as well[97,98], suggesting it supports
555 important aspects of neural function. For example, autocrine neuropeptide pathways are known to
556 mediate cell-autonomous feedback[99–104], and are therefore often suggested to maintain neuronal
557 homeostasis; this may be particularly important to regulate the activity of tonically signaling neurons,
558 such as the oxygen-sensing neurons. In the motor circuit, ostensibly autocrine signaling may play a
559 further role by coordinating the activities of neighboring neurons with similar gene expression
560 patterns. Although proprioceptive and electrical coupling between adjacent motorneurons generates
561 waves of muscle contraction over adjacent body regions[88], autocrine pathways also have the capacity
562 to coordinate physiology across neighboring cells[105,106]. Indeed, mutants for several of the
563 neuropeptide ligands that act in motorneuron autocrine pathways have been shown to have

564 locomotion defects[107,108], suggesting an important role for these connections in patterning locomotor
565 behavior.

566 We also observe a critical role for neuropeptide signaling in linking disconnected components
567 of the nervous system to the broader network. In particular, the pharyngeal neurons, which form a
568 wired network analogous (if not homologous) to the vertebrate's enteric nervous system, and the CAN
569 neurons, whose processes lie in the excretory canal-associated nerve, are virtually completely
570 unconnected to the somatic synaptic and gap junction connectomes yet are extensively integrated into
571 the neuropeptide connectome. Both CAN and the pharyngeal neurons express multiple GPCRs whose
572 ligands are expressed exclusively outside the pharynx or canal-associated nerve, indicating that these
573 neurons are regulated by peptides released from physically-unconnected processes. Despite their
574 disconnection from the wired connectomes, the pharynx and CAN neurons carry out essential
575 physiological functions; indeed, CAN and the pharyngeal neuron M4 are the only neurons whose
576 ablation is lethal to the animal[109,110]. This provides a means for communication between the wider
577 nervous system and these isolated but biologically critical neurons.

578 **Prospects for future mapping of wireless brain connectomes**

579 We have described here the draft neuropeptide connectome of *C. elegans*, an animal with 302
580 neurons. In the future, we plan to refine this connectome, for example by expanding its scope through
581 deorphanization of neuropeptide receptors whose ligands are currently unknown. Differential
582 posttranscriptional processing may also lead to the synthesis of different peptides and receptors in
583 neurons that express the same gene, and alternative patterns of gene expression during development or
584 in response to environmental cues may likewise alter the structure and function of neuropeptide
585 signaling networks. Moreover, non-neuronal cells function as both senders and receivers of
586 neuropeptide signals; with the use of reporter lines for peptides and receptors it should be possible in
587 the future to incorporate these cells into the neuropeptide connectome and observe plasticity in the
588 network. We likewise plan to integrate functional information into the connectome map; for example,
589 in vitro experiments could identify the G-protein pathways downstream of individual receptors, and *in*
590 *vivo* sensors could provide empirical data on the spatial scope of neuropeptide signaling pathways.

591 Together these data will facilitate functional modeling of neuropeptidergic circuits revealed in the
592 connectome maps.
593 In principle, the approaches described here should also be applicable to mapping the
594 neuropeptide signaling networks of animals with much larger brains. Single-cell RNAseq data from
595 different vertebrate animals indicates that, as in *C. elegans*, most neurons express at least one
596 neuropeptide precursor and at least one neuropeptide receptor, facilitating dense and potentially
597 decentralized networks[18,39,43,44]. Although it is currently not possible to precisely link gene expression
598 clusters with individual neurons in brain circuits, the use of targeted reporters should eventually make
599 it possible to relate neuropeptide and receptor expression to increasingly detailed synaptic
600 connectome maps in flies and mice. Basic mechanisms of neuropeptide signaling are shared in all
601 animals, from nematodes to mammals: neuropeptides are released from dense core vesicles and
602 diffuse across space to neurons unconnected to the releasing cell by wired synapses. And although the
603 *C. elegans* nervous system is anatomically small, at the molecular level its neuropeptide systems are
604 highly complex and show significant homology to other animals. Thus, the neuropeptide connectome
605 of *C. elegans* may serve as a prototype to unravel general principles of neuromodulatory network
606 structure that also apply to much larger brains.
607 [34,35363718,38]
608
609
610 **Methods**
611 **Reporter Transgenic Strains**
612 *CRISPR based constructs*: Thirty-two transcriptional C-terminal GFP reporters of neuropeptides and
613 neuropeptide receptors were created where GFP was recombineered in the last coding exon of the
614 gene of interest. Of the 17 total neuropeptide precursor genes that we made reporters for, 8 had only a
615 T2A::3xNLS::GFP tag, 1 had a T2A::GFP::H2B tag, 6 had both T2A::3xNLS::GFP and
616 SL2::GFP::H2B tags, and 2 had only an SL2::GFP::H2B tag (Supplementary Table 1). For the GPCR

617 receptors, 8 gene expression reporters were made all with SL2::GFP::H2B tags (Supplementary Table
618 2). Most of these constructs were made by SUNY Biotech.
619
620 **Reporter Analysis**
621 Young adult animals were mounted on 5% agarose pads and immobilized with 100 mM sodium azide
622 and imaged on a Zeiss LSM880 using a 40X objective lens. GFP expression reporters were identified
623 at single neuron resolution as described[111]. GFP reporter expression of these constructs, as reported in
624 Table S1-2 were noted using three categories: moderate to high expression, low and variable
625 expression, and no detected expression. Additionally, we compared our GFP reporter expression data
626 to single-cell RNA-seq expression (scRNAseq) data from the CeNGEN project using their standard
627 thresholds (4 being the most stringent, 1 being the least stringent, and blank be unfiltered)[40].
628 In our analysis, for each gene and each CeNGEN threshold, we tallied 1) the number of neurons that
629 showed GFP expression but not scRNA expression, 2) the number of neurons showing both GFP
630 expression and scRNA expression, and 3) the number of neurons that showed scRNA expression but
631 no GFP expression (Table S3).
632 Based on the results of this analysis threshold 4, although in some occasions too conservative, had the
633 best correlation between GFP reporter and CeNGEN scRNAseq data expression per neuron for the
634 tested NPP and GPCR genes.
635
636 **Synaptic and gap junction networks**
637 The synaptic and gap junction networks used in this work were based on the full
638 hermaphrodite *C. elegans* connectome, containing all 302 neurons. This network was composed from
639 the somatic connectome[48], updated and released by the Chklovskii lab[47]; and the pharyngeal network
640 of Albertson and Thomson[65], made available by the Cybernetic *Caenorhabditis elegans* Program
641 (CCeP). The functional classifications referred to in the text (i.e., *sensory*
642 *neuron*, *interneuron*, *motorneuron*) are based on the classification scheme used in WormAtlas[112].
643 When there is double or triple classification in nerve ring neurons that can be sensory neurons,
644 interneurons, or motorneurons, the Zhen lab classification[66] was used to select one neuron type. URB

645 left and right neurons are the only ones in which the WormAtlas and the Zhen lab classification
646 diverge, leading us to classify them as sensory neuron following the later most recent classification.
647 DB neurons are identified as motorneurons although WormAtlas indicates that these could also be
648 interneurons[112]. The gap junction network was modelled as an undirected network with bidirectional
649 electrical synapses; note however that some gap junctions might be rectifying and thus exhibit
650 directionality. In the synaptic network reciprocal connections between nodes are considered as two
651 separate unidirectional connections.
652
653 **Monoamine network construction**
654 The monoamine network used in this work was made following the same procedure as in (Bentley et
655 al., 2016). The monoamine expression for the 302 neurons comes from the neurotransmitter atlas of
656 *C. elegans*[75] and receptor expression for the 302 neurons comes from the single-cell expression data
657 from the CeNGEN project (https://www.cengen.org)[40]. We used the expression data at CeNGEN
658 threshold 4. The interactions between ligand and receptors were previously described[45]. The
659 adjacency matrix was built using a binary version of the expression data for the 302 neurons. For a
660 given point $A^M(i,j)$ and for a given monoamine receptor pair M the connection between two neurons is
661 defined by $A^M(i,j) = Mon^M(i,j) \times Receptor^M(i,j)$. Each monoamine receptor interaction forms an
662 individual binary network. To get the overall monoamines network we add each individual
663 monoamine receptor network resulting in a weighted network where the weight indicates the number
664 of monoamine receptor pairs that connect two nodes. Reciprocal connections between nodes are
665 considered as two separate unidirectional connections.
666
667 **Neuropeptide network construction**
668 The neuropeptide network used in this work was made using a similar approach to that used for the
669 monoamines. The interactions between ligands and receptors were identified using a large-scale *in*
670 *vitro* reverse pharmacology pipeline in which over 87% of the predicted peptide GPCRs were
671 challenged with FMRFamide related peptides (FLP) and non-insulin non-FLP like peptides (NLP)[64].
672 Neuropeptide precursor and GPCR gene expression for the 302 neurons was extracted from the

673 single-cell transcriptome data of the CeNGEN project (https://www.cengen.org)[40]. We used the
674 expression data at CeNGEN threshold 4. The adjacency matrix was built using a binary version of the
675 expression data for the 302 neurons. For a given point $A^N(i,j)$ and for a given neuropeptide receptor
676 pair N the connection between two neurons is defined by $A^N(i,j) = NPP^N(i,j) \times GPCR^N(i,j)$. Each
677 neuropeptide receptor interaction forms an individual binary network. To get the overall
678 neuropeptides network we add each individual neuropeptide receptor network resulting in a weighted
679 network where the weight indicates the number of neuropeptide receptor pairs that connect two nodes.
680 Reciprocal connections between nodes are considered as two separate unidirectional connections.
681

682 **Neuropeptide network spatial constraining**

683 Neuropeptidergic networks were locally thresholded to filter out connections between neurons that
684 were anatomically far from each other. The anatomical EM data was obtained from The Mind of the
685 worm (https://www.wormatlas.org/MoW_built0.92/MoW.html) and other literature[48,65,66]. This data
686 was used to create a table of locations for each neuronal process, identifying 27 different neuronal
687 process bundles in the *C. elegans* nervous system as previously defined[48]. This classification was then
688 used to filter out neuropeptidergic connections based on putative signaling ranges. The stringent
689 short-range thresholding allows connections only in between neuronal processes that are in the same
690 process bundle and the pharynx is a separated system were all connections are allowed in between
691 pharyngeal neurons only. The mid-range stringency thresholding allows connections between neurons
692 with neuronal processes in the same anatomical area: head (including pharynx and the ventral cord
693 neurons that are in the ventral ganglion), midbody and tail. And in the unthresholded system all
694 neuropeptidergic connections are allowed.
695

696 **Topological network measures**

697 Edge counts, adjacency matrices and reducibility clusters were all computed using binary directed
698 versions of the networks. The same networks, excluding self-connections (i.e. setting all diagonal
699 elements to 0), were used to compute all other measures.

Network measures are compared to 100 null model networks generated using the degree-preserving edge swap procedure from the Brain Connectivity Toolbox for MATLAB[113]. This is performed by selecting a pair of edges ($A \rightarrow B$) ($C \rightarrow D$) and swapping them to give ($A \rightarrow D$)($C \rightarrow B$). If the resulting edges already exist in the network, another pair of edges is selected instead. Each edge was swapped 10 times to ensure full randomization.

Degree

Degree is the number of edges connected to a given node. Indegree is the number of incoming connections connected to a given node and outdegree is the number of outgoing connections.

Density

Density d is the fraction of present connections K to possible connections between the given nodes N:

$$d = \frac{K}{N^2 - N}$$

Clustering coefficient

Transitivity defines the ratio of triangles to triplets in the network (where a triple is a single node with edges running to an unordered pair of others, and a triangle is a fully-connected triple). For a directed network, this is equivalent to: $T = \frac{\sum_{i \in N} t_i}{\sum_{i \in N} [(k_i^{out} + k_i^{in})(k_i^{out} + k_i^{in} - 1) - 2\sum_{j \in N} A_{ij} A_{ji}]}$ where A is the adjacency matrix, N is the number of nodes, k^{out} and k^{in} are the out-degree and in-degree, and t_i is the number of triangles around a node: $t_i = \frac{1}{2} \sum_{j,h \in N} (A_{ij} + A_{ji})\,(A_{ih} + A_{hi})(A_{jh} + A_{hj})$

Reciprocity

Reciprocity is the fraction of reciprocal edges in the network: $r = \frac{|E^{\leftrightarrow}|}{M}$ where M is the number of edges, and $|E^{\leftrightarrow}|$ is the number of reciprocal edges: $|E^{\leftrightarrow}| = \sum_{i \neq j} A_{ij} A_{ji}$

Rich-club coefficient

724 The rich-club coefficient measures the tendency for high-degree nodes in a network to form highly
725 interconnected communities[55]. These communities can be identified by creating subnetworks for each
726 degree level k and removing nodes with a degree $\leq k$. Then the rich-club coefficient $\Phi(k)$ for each
727 subnetwork is defined as the ratio of connections in the subnetwork M_k to the number of maximum
728 possible connections. For a directed network with no self-connections, where N_k is the number of
729 remaining nodes, this is given by: $\Phi(k) = \frac{M_k}{N_k(N_k - 1)}$
730 Thus, a fully connected subnetwork at a given degree k has a rich-club coefficient $\Phi(k) = 1$. We
731 normalize the rich-club coefficient by calculating: $\Phi_{norm}(k) = \frac{\Phi(k)}{\langle \Phi_{random}(k) \rangle}$ were $<\Phi_{random}(k)>$ is the
732 average value of the rich-club coefficient across random networks.
733 A rich-club exists when $\Phi_{norm}(k) \geq 1$, but in order to get a clear threshold range we use a probabilistic
734 approach. The threshold range of the rich-club is defined by $\Phi_{norm}(k) \geq 1 + 1\sigma$, where σ is the Standard
735 Deviation of $\Phi_{random}(k)$ for the 100 random networks.
736
737 **Dimensionality reduction analysis**
738 t-SNE is an algorithm for dimensionality reduction that facilitates visualizing high dimensionality
739 data. The analysis described here was performed using the MATLAB *t-sne* function on the adjacency
740 network of connections. The neuropeptide dimension was reduced, and clustering was performed
741 based on the pattern of connections due to receptor expression. Different distant measures were tested
742 to confirm the clustering: Euclidean distance, Chebychev distance, cosine distance and Mahalanobis
743 distance.
744
745 **Co-expression analysis**
746 The signaling networks used in this work represent connections between co-occurring genes. Nodes
747 are defined as pairs of neuropeptide precursor and GPCR genes that co-occur more than expected by
748 chance as measured by a Fisher's exact test[114] with FDR (false positive rate) correction[115]. The 2x2
749 contingency table for the Fisher's exact test contains the number of neurons for which both genes co-

750 occur and the number of neurons in which each NPP and GPCR gene is expressed without co-
751 occurring with the second gene. Thus, the Fisher's test is defined as:

752 $$p = \frac{(R_1!\,R_2!)(C_1!\,C_2!)}{N!\prod_{i,j} n_{i,j}!}$$

753
754 Where R_1 and R_2 are the row sums, C_1 and C_2 are the column sums, N is the total number of
755 observations in the contingency table, and n_{ij} is the value in the *i*th row and *j*th column of the table
756 Interactions between nodes are defined by the receptor-ligand interactions that the co-occurring genes
757 have with genes that co-occur in another node. The interactions between ligand and receptors were
758 identified using a large-scale *in vitro* reverse pharmacology pipeline[64].
759

760 **Software**

761 Network measures were computed in MATLAB (v9.8.0.1323502 (R2020a), The MathWorks Inc.
762 Natick, MA) using the Brain Connectivity Toolbox[113] (v2019-03-03) and the MATLAB/Octave
763 Networks Toolbox[116]. Clustering and visualization of multilayer plots was performed using
764 MuxViz[117]. And additional network visualizations were created using Cytoscape[118].
765

766 **Lead contact**

767 Requests for resources should be directed to the Lead Contact William Schafer (wschafer@mrc-
768 lmb.cam.ac.uk)
769

770 **Data and software availability**

771 The scRNAseq data are available at www.cengen.org. The biochemical deorphanization data are
772 available at https://worm.peptide-gpcr.org/project/neuropeptides/flps/ [64]. Analysis code is available at
773 GitHub

774 **Nematode Strains**

775 The strains used in this study are listed in Supplementary Tables 1 and 2.
776

Acknowledgements

This work was funded by grants from NIH (R01NS110391, to OH, WRS and IB), the MRC (MC-A023-5PB91, to WRS), the Wellcome Trust (WT103784MA, to WRS), MQ: Transforming Mental Health (MQF17_24, to PV) the ERC (950328, to IB), HHMI (to OH), and the Simons Foundation (855199, to RF). This research was also supported in part by the NIHR Cambridge Biomedical Research Centre (BRC-1215-20014) and NIHR Applied Research Centre. The views expressed are those of the author(s) and not necessarily those of any funding bodies. For the purpose of open access, the authors have applied a Creative Commons Attribution (CC BY) license to any Author Accepted Manuscript version arising from this submission.

We'd like to thank the LMB Visual Aids and Scientific Computing teams for their support, especially Johanna Westmorland for figure 3 design. We thank Tom Shimizu, Erik Larsson Lekholm, Mark Moyle, Caroline Nettekoven, Sarah Morgan, Albert Cardona, Ed Bullmore, Amy Courtney and Mei Zhen for productive discussions. We thank WormAtlas, OpenWorm, Nemanode and WormBase for their resources.

Author contributions

L.R.S., W.R.S., P.E.V., J.W. and I.B. designed research. L.R.S. and J.W. performed analysis. H.S. and R.F. made strains and interpreted images. H.S., R.F., S.R.T., A.W., M.H., D.M.M., O.H. contributed with data and discussion. L.R.S., W.R.S., P.E.V., J.W. and I.B. contributed to writing the paper. All authors reviewed and approved the manuscript.

Declaration of Interests

The authors declare no competing interests

Figure titles and Legends

Figure 1. *In silico* reconstruction of the neuropeptidergic connectome of the *C. elegans* nervous system by combining *in vitro* neuropeptide-GPCR interaction, gene expression and anatomical datasets.

(A) Datasets used to build the network *in silico.* Left: biochemical neuropeptide-GPCR interaction dataset defining 91 neuropeptide - G protein-coupled receptor (GPCR) pairs below

805 500 nM EC_{50} affinity, coupling 51 GPCRs to 48 neuropeptides[64]. Neuropeptides from the
806 same precursor gene (NPP) are considered the same. Middle: anatomical and morphological
807 description of the *C. elegans* hermaphrodite nervous system[48]. Right: single-cell RNAseq
808 expression of the 302 *C. elegans* neurons, adapted from[40].
809 (B) Representation of the *C. elegans* nervous system connectome network in which all types of
810 neurons (pharyngeal, interneuron, CAN neurons, motorneurons and sensory neurons) are
811 connected through neuropeptidergic connections.
812
813 **Figure 2**. Single-copy genomic knock-in reporters corroborate the scRNAseq expression profiles of
814 several neuropeptide and GPCR genes. GFP-positive neurons were identified using the NeuroPAL
815 multicolor transgene [111]Figure pictures all segments (head, tail, vulva and midbody) showing neuronal
816 expression, within which individual neurons are circled and labeled. Scale bars represent 10 µm
817 (A) Fluorescent GFP reporters for the expression of 17 representative neuropeptide precursor
818 genes.
819 (B) Fluorescent GFP reporters for the expression of 8 representative GPCR precursor genes.
820 Images of the *trhr-1* expression strain show some bleed-through signal that does not represent
821 neuronal expression.
822
823 **Figure 3**. Analysis of neuropeptide and receptor expression allows assessment of the spatial scale of
824 neuropeptide signaling.
825 (A) Full anatomical description of the *C. elegans* hermaphrodite nervous system[112]. Neuronal
826 bundles represented in red, and the pharynx in green. Short-range connections are defined as
827 occurring within the same neuronal bundle (axons and dendrites considered equally). Mid-
828 range connections occur between neurons whose processes are present in one of following
829 distinct anatomical areas: head (ranging from nose to deirid commissures including the
830 ventral and retrovesicular ganglion), midbody (between but not including deirid commissures
831 and the preanal ganglion), or tail (from and including the preanal ganglion to the tail's tip).

832 (B) Expression matrix for 23 GPCRs activated *in vitro* by a single neuropeptide ligand. Neurons
833 are sorted by neuron type on the x axis and the expression of each GPCR on the y axis. Colors
834 indicate the range of diffusion distance required for communication with at least one ligand-
835 expressing neuron: blue indicates that the receptor expressing neuron makes contact with a
836 neuron expressing its ligand, either within the same stratum of the nerve ring (dark blue) or in
837 a thinner neuronal bundle (light blue); orange indicates short-range connections between
838 strata in the nerve ring (i.e. between neurons in same bundle but not in physical contact); red
839 indicates connections between neurons in the same anatomical area but not in the same
840 bundle. Nerve ring stratum as defined[67,6867,6867,68]
841 (C) Expression matrix for 23 neuropeptide precursor genes with a single target receptor in vitro.
842 Neurons are sorted by neuron type on the x axis and the expression of each neuropeptide gene
843 on the y axis. Colors indicate the range of diffusion distance required for communication with
844 a receptor-expressing neuron, as described above.
845 **Figure 4**. Assortativity analysis of 91 individual NPP-GPCR networks shows different topologies
846 depending on the NPP-GPCR interaction.
847 (A) Representation of network topologies depending on assortativity, reflecting the preference of
848 neuropeptides to signal to GPCRs that are expressed in the same number of neurons.
849 Networks are classified either as local, pervasive, broadcaster or integrative. Bottom left:
850 scatter plot showing the number of neurons expressing a particular GPCR versus the number
851 of neurons expressing the corresponding NPP gene for each of the 91 individual networks.
852 Local networks show restricted NPP and GPCR expression in 50 neurons or less. Pervasive
853 networks have broad NPP and GPCR expression in more than 50 neurons. Broadcaster
854 networks show broad GPCR (>50 neurons) but restricted NPP expression (≤50 neurons),
855 while integrative networks display broad NPP (>50 neurons) and restricted GPCR expression
856 (≤50 neurons). Filled circles indicate receptor presence in that neuron and empty circles
857 indicate neuropeptide release from that neuron. Representative NPP-GPCR networks
858 highlighting prototypical assortivities.. Left top: example of local network for CAPA-
859 1/NMUR-1 that has been linked to learning[32]. Left middle top: example of pervasive network

860 FLP-18/NPR-5 of which the receptor is implicated within locomotory behavior[119]. Right
861 middle top: example of broadcaster network FLP-1/FRPR-7 that modulates the interaction
862 between food sensation and locomotion[13]. Right top: example of integrative network NLP-
863 47/GNRR-1, the receptor of which is linked to egg-laying behavior [120] and is only activated by
864 NLP-47 *in vitro* [64,120]. [120]
865 (B) The topology of the network is defined by the individual NPP-GPCR pairing. Networks of the
866 same receptor can show different topologies depending on its neuropeptide ligand. .
867
868 **Figure 5**. The aggregate neuropeptide connectome in *C. elegans* connects all 302 neurons in a dense
869 network.
870 Adjacency matrix representation of the aggregate 91 NPP-GPCR pair network considering short-
871 range (color) and mid-range (gray) diffusion models. Axes represent the number of NPP and GPCR
872 genes per neuron. Virtually all neurons express at least 1 NPP and 1 GPCR gene, the only exception
873 of which is the IL1 neuron class that does not show GPCR expression. Neurons can communicate
874 with each other using up to 18 different NPP-GPCR pathways, a feature conserved in both short- and
875 mid-range diffusion models. Dense and diverse connections are mainly seen from oxygen sensing
876 neurons to inter- and motorneurons. 5% of all connections are putative autocrine connections in which
877 a single neuron co-expresses both NPP and GPCR genes of a cognate pair.
878
879 **Figure 6**. Topological analysis of the *C. elegans* nervous system highlights neuropeptide signaling
880 hubs and a large rich club.
881 (A) Degree distribution of the short-range model aggregate neuropeptide network. Degree (sum of
882 incoming and outgoing connections) is shown in orange, the indegree (sum of incoming
883 connections) is shown in green and the outdegree (sum of outgoing connections) is shown in
884 purple. . The 10 hubs with the highest degree are indicated, including hubs of the synaptic
885 connectome (AVAL/R, PVCL/R and DVA) as well as 6 neurons with specialised roles in the
886 neuropeptide signaling network (AVKL/R, PVT, PVQL/R, PVR).

887 (B) Degree distribution of the mid-range model aggregate neuropeptide network. Similar to the
888 short-range model, degree distribution is equally influenced by both in- and outdegree: the 10
889 hub neurons of highest degree are indicated.
890 (C) Degree distribution of the synaptic network of *C. elegans*. Compared to the neuropeptide
891 connectome, the synaptic connectome contains a much smaller number of high-degree hub
892 nodes.
893 (D) Degree distribution of the monoamine network of *C. elegans.* The overall degree distribution
894 shows two distinct phases, correlating with the network having a star-like topology centered
895 around a small core of high degree hubs. This topological feature is further reflected in the
896 low outdegree of most neurons.
897 (E) Conceptual network representation highlighting: node (neuron), edge (connection between
898 neurons), degree (k, sum of incoming and outgoing connections), hub (highly connected
899 neurons), and rich club (group of hubs that connect more to one another than to the rest of the
900 network).
901 (F) Rich club of the *C. elegans* neuropeptidergic connectome. The rich club coefficient $\Phi(k)$ for
902 the *C. elegans* neuropeptidergic network is shown in black and the randomized rich club
903 curve $\Phi_{random}(k)$ generated by averaging the rich club coefficients of 100 randomized versions
904 of the *C. elegans* neuropeptidergic network that preserve degree distribution) is depicted in
905 gray. The red curve is the normalized coefficient. $\Phi(k) \geq \Phi_{random}(k) + 10\sigma$ over the range 203
906 $\leq k \leq 298$, indicating the rich club. The large number of connections in the range $k > 298$
907 make the random networks more unreliable but since $\Phi(k)$ is very close and mostly higher
908 than $\Phi_{random}(k) + 10\sigma$ we can infer that all neurons where $203 \leq k$ are part of the rich club.
909 This means the short-range aggregate neuropeptide network has a rich club of 156 neurons
910 (166 in the mid-range, Suppl. Figure 6)
911 (G) Correlation between synaptic and neuropeptidergic degrees. A positive correlation was
912 observed over all neurons ($r = 0.54$, $p = 3.1\ e^{-14}$). Dark red dots indicate neurons in the *C.*
913 *elegans* neuropeptidergic rich club. Synaptic hubs, which also exhibit a high neuropeptide

914 degree (k>400) (ranking among the top 30 neuropeptide hubs) are highlighted. Also
915 highlighet are 6 neuropeptidergic hubs, with low synaptic degree (k < 30, below the
916 correlation line), as well as low monoamine (22 > k ≥ 10) and gap junction (14 > k ≥ 3)
917 degrees (Suppl. Figure 6), appear to be specialized for neuropeptide signaling.
918
919 **Figure 7**. Mesoscale structure of the neuropeptide connectome
920 (A) t-SNE dimensionality reduction of the adjacency matrix of the mid-range aggregate network
921 (Euclidean distance, perplexity 30). This plot we identifies 3 clear clusters (1, 2, 3) which
922 encompass 112 of out the 166 mid-range neuropeptide rich club neurons), in addition to a
923 periphery of loosely clustered neurons. Datapoint markers represent their neuronal
924 classification.
925 (B) PCA dimensionality reduction of the adjacency matrix of the mid-range aggregate network
926 (Euclidean distance, perplexity 30). Neurons in this plot are colored based on that of the
927 groups defined in (A). A clustering pattern similar to that following t-SNE appears,
928 highlighting the robustness of these defined groups across dimensionality reduction
929 techniques. Datapoint markers represent their neuronal classification.
930 (C) Mid-range aggregate network sorted in both dimensions (sending and receiving neurons)
931 based on neuronal clusters defined in (A) and (B). Neuronal clusters divisions are highlighted
932 with discontinuous lines. Group 3 does not receive nor send connections to group 1. All three
933 groups, specially 2 and 3, send a large number of connections to peripheral neurons while not
934 receiving significant input from the periphery. Group 2 is the only group that sends and
935 receives connections to and from all 4 neuronal clusters. The neurons with higher weight of
936 connections (number of NPP-GPCR pairs used to make the connection) are mainly found in
937 groups 2 and 3. The neurons defining the patterns that drive the clustering of each group are
938 shown at the bottom: group 1 is mainly driven by the connections of DA, VC and VA
939 terminal motorneurons; group 2 is mainly driven by the connections of neuropeptidergic hubs
940 PVQL/R and PVR, synaptic hubs AVAL/R and PVNL/R neurons; group 3 is mainly driven
941 by the connections of pharyngeal neurons I5 and I4 and RIR, RICL/R interneurons.

942 (D) Violin plots showing indegree values for the 3 clusters and the periphery. Indegree cleanly
943 defines the 3 groups and the periphery (median group 1: 139, median group 2: 267, median
944 group 3: 198, median periphery: 54), and therefore is the determinant factor in the definition
945 of these groups. Significances determined by Kruskal-Wallis test followed by Tukey-Kramer
946 test for multiple comparisons with rank sums. The mean ranks for the 4 groups were shown to
947 be significantly different (mean rank group 1: 162, mean rank group 2: 276, mean rank group
948 3: 223, mean rank periphery: 77). n.s. not significant; ***$p \leq 0.001$.
949 (E) Diagram showing the organization of connections between the 3 defined clusters. Group 1
950 contains the main motorneurons core. These connect between themselves, with the periphery
951 and with group 2. Group 2 contains the main interneurons core including the top 10 hubs.
952 These neurons connect to almost every other neuron in the nervous system. Group 3 contains
953 the main sensory neurons and pharyngeal neurons core. These neurons connect to group 2
954 neurons and the periphery but do not connect to group 1 neurons. This structure indicates an
955 intrinsic organization of the *C. elegans* neuropeptidergic connectome rich club and how it
956 coordinates the function of the overall neuropeptidergic connectome.
957
958 **Figure 8**. Co-expression between GPCRs and their corresponding neuropeptide ligand(s) facilitates
959 potential autocrine and paracrine signaling.
960 (A) Neuronal expression matrix for both NPP and GPCR genes of the 91 NPP-GPCR pairs. Grey
961 dots represent neuronal expression of only the NPP (upper panel) or GPCR (lower panel)
962 gene, which black dots indicating co-expression of both.
963 (B) Percentage of each neuron type showing peptide autocrine connections (upper panel). The
964 number of different NPP-GPCR pairs being co-expressed in each neuron type is figured in the
965 bottom panel. Neurons showing the highest diversity of different NPP-GPCR pairs being co-
966 expressed are highlighted, including the sensory neurons PQR and URX and the interneuron
967 PVR.
968 (C) Scatter plot showing the number of neurons with co-expression for each of the 91 NPP-
969 GPCRs. Pairs with promiscuous GPCRs, specially DMSR-1 and DMSR-7 are co-expressed in

970 many different neurons, highlighting their central role in autocrine neuropeptidergic
971 signaling.
972 (D) Correlation between number of autocrine connections and neuropeptide (left) or synaptic
973 (right) degree for each of the 302 neurons. Point shapes indicate degree (round), indegree
974 (incoming arrow), outdegree (outgoing arrow).
975 (E) Representation of the autocrine connections in each neuron of the *C. elegans* worm (anterior
976 part of the worm in the left side, posterior in the right, dorsal upper part, and ventral lower
977 part). The size of each cell body indicates the number of autocrine NPP-GPCR pairs
978 expressed in that neuron. Circuits in which autocrine connections are prominent are the
979 locomotion and oxygen sensing circuit. The colors indicate the neurons in the oxygen sensing
980 and locomotion circuits that have the largest number of autocrine connections. Left bottom:
981 oxygen sensing circuits with autocrine connections, URX and PQR are the neurons with the
982 largest number of connections (arrow size indicates number of NPP-GPCR pairs). Right
983 bottom: description of the locomotion system with autocrine connections, VA/VB and
984 DA/DB are excitatory motorneurons that actuate worm crawling and which show many
985 autocrine connections while inhibitory DD/VD and minor excitatory AS motorneurons do not
986 have autocrine connections.
987
988 **Supplementary Figure 1.** Graphical representations of the 91 NPP-GPCR networks with short-range
989 connections. Colors given by assortativity like Figure 4; yellow indicates local, green pervasive, blue
990 integrative and red promiscuous networks.
991 **Supplementary Figure 2.** Graphical representations of the 91 NPP-GPCR networks with mid-range
992 connections. Networks are sorted in the same order as in Supplementary Figure 1 for comparison.
993 Colors given by assortativity as defined in Figure 4, yellow indicates local, green pervasive, blue
994 integrative and red promiscuous networks. Networks that change assortativity between short and mid-
995 range spatial models of neuropeptide transmission are highlighted.
996

997 **Supplementary Figure 3.** Adjacency matrix representation of the long and mid-range neuropeptide
998 networks. A) Model 1, aggregate matrix of the long-range neuropeptide connections, the histogram
999 lining the matrix indicate the number of GPCR or NPP that the neuron expresses. B) Model 2,
1000 aggregate matrix of the mid-range neuropeptide connections.
1001
1002 **Supplementary Figure 4.** Co-expression analysis of NPP-GPCR non cognate pairs. A) Hierarchical
1003 clustering matrix of the NPP vs GPCR co-expression. The y axis indicates GPCR and the x axis
1004 indicates NPP expression. The significance of their co-expression is indicated by the legend. B)
1005 Adjacency matrix representation of the co-expression network. The nodes are the neurons in which a
1006 NPP and a non-cognate GPCR co-express, the edges are formed when the NPP of one node is the
1007 ligand of the GPCR of another node. C) Hierarchical clustering matrix of the NPP vs NPP co-
1008 expression. D) Hierarchical clustering matrix of the GPCR vs. GPCR co-expression. E) Visual
1009 representation of one of the possible signaling cascades based on the co-expression network. DMSR-3
1010 co-expresses with FLP-34 and NLP-54 releasing neurons, which means that secretion could be
1011 activated by FLP-14 binding to DMSR-3.
1012
1013 **Supplementary Figure 5.** Autocrine connections sensitivity analysis. A) comparison of co-
1014 expression of cognate NPP-GPCR pairs in the 4 different combinations of CeNGEN and
1015 deorphanization datasets with different stringencies (CeNGEN threshold 2 or 4; EC_{50} threshold 1 μM
1016 or 500 nM), each depicted in a different color. B) Number of NPP-GPCR co-expressed per fraction of
1017 neurons in these 4 different combinations of datasets. C) Number of neurons with co-expression for
1018 the FLP or NLP neuropeptides show that FLP are more prevalent. D) Comparison of number of
1019 autocrine connections between specific and promiscuous NPP-GPCR pairs, showing that promiscuous
1020 pairs tend to have more autocrine connections. E) Correlation of autocrine connections with gap
1021 junction and monoamine networks. F) Number of autocrine connections in each motorneuron for each
1022 of the main promiscuous NPP-GPCR pairs present in those neurons.
1023
1024 **References**

1025 1. Eichler, K., Li, F., Litwin-Kumar, A., Park, Y., Andrade, I., Schneider-Mizell, C.M.,
1026 Saumweber, T., Huser, A., Eschbach, C., Gerber, B., et al. (2017). The complete connectome
1027 of a learning and memory centre in an insect brain. Nature *548*, 175–182.
1028 10.1038/nature23455.
1029 2. Scheffer, L.K., Xu, C.S., Januszewski, M., Lu, Z., Takemura, S., Hayworth, K.J., Huang, G.B.,
1030 Shinomiya, K., Maitlin-Shepard, J., Berg, S., et al. (2020). A connectome and analysis of the
1031 adult Drosophila central brain. Elife *9*, e57443. 10.7554/eLife.57443.
1032 3. Verasztó, C., Jasek, S., Gühmann, M., Shahidi, R., Ueda, N., Beard, J.D., Mendes, S., Heinz,
1033 K., Bezares-Calderón, L.A., Williams, E., et al. (2020). Whole-animal connectome and cell-
1034 type complement of the three-segmented *Platynereis dumerilii* larv.
1035 4. Hulse, B.K., Haberkern, H., Franconville, R., Turner-Evans, D., Takemura, S., Wolff, T.,
1036 Noorman, M., Dreher, M., Dan, C., Parekh, R., et al. (2021). A connectome of the Drosophila
1037 central complex reveals network motifs suitable for flexible navigation and context-dependent
1038 action selection. Elife *10*, e66039. 10.7554/eLife.66039.
1039 5. Ryan, K., Lu, Z., and Meinertzhagen, I.A. (2016). The CNS connectome of a tadpole larva of
1040 Ciona intestinalis (L.) highlights sidedness in the brain of a chordate sibling. Elife *5*, e16962.
1041 10.7554/eLife.16962.
1042 6. Kunst, M., Laurell, E., Mokayes, N., Kramer, A., Kubo, F., Fernandes, A.M., Förster, D., Dal
1043 Maschio, M., and Baier, H. (2019). A Cellular-Resolution Atlas of the Larval Zebrafish Brain.
1044 Neuron *103*, 21-38.e5. 10.1016/j.neuron.2019.04.034.
1045 7. Oh, S.W., Harris, J.A., Ng, L., Winslow, B., Cain, N., Mihalas, S., Wang, Q., Lau, C., Kuan,
1046 L., Henry, A.M., et al. (2014). A mesoscale connectome of the mouse brain. Nature *508*, 207–
1047 214. 10.1038/nature13186.
1048 8. Nässel, D.R. (2009). Neuropeptide signaling near and far: how localized and timed is the
1049 action of neuropeptides in brain circuits? Invertebrate Neuroscience *9*, 57–75.
1050 10.1007/s10158-009-0090-1.
1051 9. van den Pol, A.N. (2012). Neuropeptide Transmission in Brain Circuits. Neuron *76*, 98–115.
1052 10.1016/j.neuron.2012.09.014.

1053 10. Atkinson, L.E., Liu, Y., McKay, F., Vandewyer, E., Viau, C., Irvine, A., Rosa, B.A., Li, Z.,
1054 Liang, Q., Marks, N.J., et al. (2021). *Ascaris suum* Informs Extrasynaptic Volume
1055 Transmission in Nematodes. ACS Chem Neurosci *12*, 3176–3188.
1056 10.1021/acschemneuro.1c00281.
1057 11. Nurrish, S. (2014). Dense Core Vesicle Release: Controlling the Where as Well as the When.
1058 Genetics *196*, 601–604. 10.1534/genetics.113.159905.
1059 12. Marder, E. (2012). Neuromodulation of Neuronal Circuits: Back to the Future. Neuron *76*, 1–
1060 11. 10.1016/j.neuron.2012.09.010.
1061 13. Oranth, A., Schultheis, C., Tolstenkov, O., Erbguth, K., Nagpal, J., Hain, D., Brauner, M.,
1062 Wabnig, S., Costa, W.S., McWhirter, R.D., et al. (2018). Food Sensation Modulates
1063 Locomotion by Dopamine and Neuropeptide Signaling in a Distributed Neuronal Network.
1064 Neuron *100*, 1414-1428.e10. 10.1016/j.neuron.2018.10.024.
1065 14. Chew, Y.L., Tanizawa, Y., Cho, Y., Zhao, B., Yu, A.J., Ardiel, E.L., Rabinowitch, I., Bai, J.,
1066 Rankin, C.H., Lu, H., et al. (2018). An Afferent Neuropeptide System Transmits
1067 Mechanosensory Signals Triggering Sensitization and Arousal in C. elegans. Neuron *99*, 1233-
1068 1246.e6. 10.1016/j.neuron.2018.08.003.
1069 15. Lin, S., Senapati, B., and Tsao, C.-H. (2019). Neural basis of hunger-driven behaviour in
1070 Drosophila. Open Biol *9*, 180259. 10.1098/rsob.180259.
1071 16. Ramachandran, S., Banerjee, N., Bhattacharya, R., Lemons, M.L., Florman, J., Lambert, C.M.,
1072 Touroutine, D., Alexander, K., Schoofs, L., Alkema, M.J., et al. (2021). A conserved
1073 neuropeptide system links head and body motor circuits to enable adaptive behavior. Elife *10*,
1074 e71747. 10.7554/eLife.71747.
1075 17. Melzer, S., Newmark, E.R., Mizuno, G.O., Hyun, M., Philson, A.C., Quiroli, E., Righetti, B.,
1076 Gregory, M.R., Huang, K.W., Levasseur, J., et al. (2021). Bombesin-like peptide recruits
1077 disinhibitory cortical circuits and enhances fear memories. Cell *184*, 5622-5634.e25.
1078 10.1016/j.cell.2021.09.013.
1079 18. Zhong, W., Barde, S., Mitsios, N., Adori, C., Oksvold, P., Feilitzen, K. von, O'Leary, L.,
1080 Csiba, L., Hortobágyi, T., Szocsics, P., et al. (2022). The neuropeptide landscape of human

prefrontal cortex. Proceedings of the National Academy of Sciences *119*, e2123146119. 10.1073/pnas.2123146119.

19. Bargmann, C.I. (2012). Beyond the connectome: How neuromodulators shape neural circuits. BioEssays *34*, 458–465. 10.1002/bies.201100185.

20. Schoofs, L., de Loof, A., and van Hiel, M.B. (2017). Neuropeptides as Regulators of Behavior in Insects. Annu Rev Entomol *62*, 35–52. 10.1146/annurev-ento-031616-035500.

21. Bhat, U.S., Shahi, N., Surendran, S., and Babu, K. (2021). Neuropeptides and Behaviors: How Small Peptides Regulate Nervous System Function and Behavioral Outputs. Front Mol Neurosci *14*.

22. van Bael, S., Watteyne, J., Boonen, K., de Haes, W., Menschaert, G., Ringstad, N., Horvitz, H.R., Schoofs, L., Husson, S.J., and Temmerman, L. (2018). Mass spectrometric evidence for neuropeptide-amidating enzymes in. Journal of Biological Chemistry *293*, 6052–6063. 10.1074/jbc.RA117.000731.

23. Jékely, G. (2021). The chemical brain hypothesis for the origin of nervous systems. Philosophical Transactions of the Royal Society B: Biological Sciences *376*, 20190761. 10.1098/rstb.2019.0761.

24. Yañez-Guerra, L.A., Thiel, D., and Jékely, G. (2022). Premetazoan Origin of Neuropeptide Signaling. Mol Biol Evol *39*, msac051. 10.1093/molbev/msac051.

25. Frooninckx, L., van Rompay, L., Temmerman, L., van Sinay, E., Beets, I., Janssen, T., Husson, S., and Schoofs, L. (2012). Neuropeptide GPCRs in C. elegans. Front Endocrinol (Lausanne) *3*.

26. Jékely, G. (2013). Global view of the evolution and diversity of metazoan neuropeptide signaling. Proceedings of the National Academy of Sciences *110*, 8702–8707. 10.1073/pnas.1221833110.

27. Rizzo, M.J., and Johnson, E.C. (2020). Homodimerization of Drosophila Class A neuropeptide GPCRs: Evidence for conservation of GPCR dimerization throughout metazoan evolution. Biochem Biophys Res Commun *523*, 322–327. 10.1016/j.bbrc.2019.12.019.

1108 28. Rogers, C., Reale, V., Kim, K., Chatwin, H., Li, C., Evans, P., and de Bono, M. (2003).
1109 Inhibition of Caenorhabditis elegans social feeding by FMRFamide-related peptide activation
1110 of NPR-1. Nat Neurosci *6*, 1178–1185. 10.1038/nn1140.
1111 29. Beets, I., Janssen, T., Meelkop, E., Temmerman, L., Suetens, N., Rademakers, S., Jansen, G.,
1112 and Schoofs, L. (2012). Vasopressin/Oxytocin-Related Signaling Regulates Gustatory
1113 Associative Learning in *C. elegans*. Science (1979) *338*, 543–545. 10.1126/science.1226860.
1114 30. Iannacone, M.J., Beets, I., Lopes, L.E., Churgin, M.A., Fang-Yen, C., Nelson, M.D., Schoofs,
1115 L., and Raizen, D.M. (2017). The RFamide receptor DMSR-1 regulates stress-induced sleep in
1116 C. elegans. Elife *6*, e19837. 10.7554/eLife.19837.
1117 31. Nässel, D.R., and Zandawala, M. (2019). Recent advances in neuropeptide signaling in
1118 Drosophila, from genes to physiology and behavior. Prog Neurobiol *179*, 101607.
1119 10.1016/j.pneurobio.2019.02.003.
1120 32. Watteyne, J., Peymen, K., van der Auwera, P., Borghgraef, C., Vandewyer, E., van Damme,
1121 S., Rutten, I., Lammertyn, J., Jelier, R., Schoofs, L., et al. (2020). Neuromedin U signaling
1122 regulates retrieval of learned salt avoidance in a C. elegans gustatory circuit. Nat Commun *11*,
1123 2076. 10.1038/s41467-020-15964-9.
1124 33. Topilko, T., Diaz, S.L., Pacheco, C.M., Verny, F., Rousseau, C. v, Kirst, C., Deleuze, C.,
1125 Gaspar, P., and Renier, N. (2022). Edinger-Westphal peptidergic neurons enable maternal
1126 preparatory nesting. Neuron *110*, 1385-1399.e8. 10.1016/j.neuron.2022.01.012.
1127 34. Davenport, A.P., Scully, C.C.G., de Graaf, C., Brown, A.J.H., and Maguire, J.J. (2020).
1128 Advances in therapeutic peptides targeting G protein-coupled receptors. Nat Rev Drug Discov
1129 *19*, 389–413. 10.1038/s41573-020-0062-z.
1130 35. Coleman, P.J., Gotter, A.L., Herring, W.J., Winrow, C.J., and Renger, J.J. (2017). The
1131 Discovery of Suvorexant, the First Orexin Receptor Drug for Insomnia. Annu Rev Pharmacol
1132 Toxicol *57*, 509–533. 10.1146/annurev-pharmtox-010716-104837.
1133 36. Hargreaves, R., Ferreira, J.C.A., Hughes, D., Brands, J., Hale, J., Mattson, B., and Mills, S.
1134 (2011). Development of aprepitant, the first neurokinin-1 receptor antagonist for the

1135 prevention of chemotherapy-induced nausea and vomiting. Ann N Y Acad Sci *1222*, 40–48.
1136 10.1111/j.1749-6632.2011.05961.x.
1137 37. Zhang, Z.Q., and Hölscher, C. (2020). GIP has neuroprotective effects in Alzheimer and
1138 Parkinson's disease models. Peptides (N.Y.) *125*, 170184. 10.1016/j.peptides.2019.170184.
1139 38. Hoyer, D., and Bartfai, T. (2012). Neuropeptides and Neuropeptide Receptors: Drug Targets,
1140 and Peptide and Non-Peptide Ligands: a Tribute to Prof. Dieter Seebach. Chem Biodivers *9*,
1141 2367–2387. 10.1002/cbdv.201200288.
1142 39. Yao, Z., van Velthoven, C.T.J., Nguyen, T.N., Goldy, J., Sedeno-Cortes, A.E., Baftizadeh, F.,
1143 Bertagnolli, D., Casper, T., Chiang, M., Crichton, K., et al. (2021). A taxonomy of
1144 transcriptomic cell types across the isocortex and hippocampal formation. Cell *184*, 3222-
1145 3241.e26. 10.1016/j.cell.2021.04.021.
1146 40. Taylor, S.R., Santpere, G., Weinreb, A., Barrett, A., Reilly, M.B., Xu, C., Varol, E.,
1147 Oikonomou, P., Glenwinkel, L., McWhirter, R., et al. (2021). Molecular topography of an
1148 entire nervous system. Cell *184*, 4329-4347.e23. 10.1016/j.cell.2021.06.023.
1149 41. Li, H., Janssens, J., de Waegeneer, M., Kolluru, S.S., Davie, K., Gardeux, V., Saelens, W.,
1150 David, F.P.A., Brbić, M., Spanier, K., et al. (2022). Fly Cell Atlas: A single-nucleus
1151 transcriptomic atlas of the adult fruit fly. Science (1979) *375*, eabk2432.
1152 10.1126/science.abk2432.
1153 42. Tasic, B., Yao, Z., Graybuck, L.T., Smith, K.A., Nguyen, T.N., Bertagnolli, D., Goldy, J.,
1154 Garren, E., Economo, M.N., Viswanathan, S., et al. (2018). Shared and distinct transcriptomic
1155 cell types across neocortical areas. Nature *563*, 72–78. 10.1038/s41586-018-0654-5.
1156 43. Smith, S.J., Sümbül, U., Graybuck, L.T., Collman, F., Seshamani, S., Gala, R., Gliko, O.,
1157 Elabbady, L., Miller, J.A., Bakken, T.E., et al. (2019). Single-cell transcriptomic evidence for
1158 dense intracortical neuropeptide networks. Elife *8*, e47889. 10.7554/eLife.47889.
1159 44. Smith, S.J. (2021). Transcriptomic evidence for dense peptidergic networks within forebrains
1160 of four widely divergent tetrapods. Curr Opin Neurobiol *71*, 100–109.
1161 10.1016/j.conb.2021.09.011.

45. Bentley, B., Branicky, R., Barnes, C.L., Chew, Y.L., Yemini, E., Bullmore, E.T., Vértes, P.E., and Schafer, W.R. (2016). The Multilayer Connectome of Caenorhabditis elegans. PLoS Comput Biol *12*, e1005283. 10.1371/journal.pcbi.1005283.

46. Cook, S.J., Jarrell, T.A., Brittin, C.A., Wang, Y., Bloniarz, A.E., Yakovlev, M.A., Nguyen, K.C.Q., Tang, L.T.-H., Bayer, E.A., Duerr, J.S., et al. (2019). Whole-animal connectomes of both Caenorhabditis elegans sexes. Nature *571*, 63–71. 10.1038/s41586-019-1352-7.

47. Varshney, L.R., Chen, B.L., Paniagua, E., Hall, D.H., and Chklovskii, D.B. (2011). Structural Properties of the Caenorhabditis elegans Neuronal Network. PLoS Comput Biol *7*, e1001066. 10.1371/journal.pcbi.1001066.

48. White, J.G., Southgate, E., Thomson, J.N., and Brenner, S. (1986). The structure of the nervous system of the nematode *Caenorhabditis elegans*. Philosophical Transactions of the Royal Society of London. B, Biological Sciences *314*, 1–340. 10.1098/rstb.1986.0056.

49. Watts, D.J., and Strogatz, S.H. (1998). Collective dynamics of 'small-world' networks. *393*, 3.

50. Bassett, D.S., and Bullmore, E.T. (2017). Small-World Brain Networks Revisited. The Neuroscientist *23*, 499–516. 10.1177/1073858416667720.

51. Reigl, M., Alon, U., and Chklovskii, D.B. (2004). Search for computational modules in the C. elegans brain. BMC Biol *2*, 25. 10.1186/1741-7007-2-25.

52. Pavlovic, D.M., Vértes, P.E., Bullmore, E.T., Schafer, W.R., and Nichols, T.E. (2014). Stochastic Blockmodeling of the Modules and Core of the Caenorhabditis elegans Connectome. PLoS One *9*, e97584. 10.1371/journal.pone.0097584.

53. Pathak, A., Chatterjee, N., and Sinha, S. (2020). Developmental trajectory of Caenorhabditis elegans nervous system governs its structural organization. PLoS Comput Biol *16*, e1007602. 10.1371/journal.pcbi.1007602.

54. Helm, A., Blevins, A.S., and Bassett, D.S. (2021). The growing topology of the C. elegans connectome (bioRxiv).

55. Towlson, E.K., Vertes, P.E., Ahnert, S.E., Schafer, W.R., and Bullmore, E.T. (2013). The Rich Club of the C. elegans Neuronal Connectome. Journal of Neuroscience *33*, 6380–6387. 10.1523/JNEUROSCI.3784-12.2013.

1190 56. van den Heuvel, M.P., and Sporns, O. (2011). Rich-Club Organization of the Human
1191 Connectome. Journal of Neuroscience *31*, 15775–15786. 10.1523/JNEUROSCI.3539-11.2011.
1192 57. Schroeter, M.S., Charlesworth, P., Kitzbichler, M.G., Paulsen, O., and Bullmore, E.T. (2015).
1193 Emergence of Rich-Club Topology and Coordinated Dynamics in Development of
1194 Hippocampal Functional Networks In Vitro. Journal of Neuroscience *35*, 5459–5470.
1195 10.1523/JNEUROSCI.4259-14.2015.
1196 58. Milo, R., Shen-Orr, S., Itzkovitz, S., Kashtan, N., Chklovskii, D., and Alon, U. (2002).
1197 Network Motifs: Simple Building Blocks of Complex Networks. Science (1979) *298*, 824–
1198 827. 10.1126/science.298.5594.824.
1199 59. Alon, U. (2007). Network motifs: theory and experimental approaches. Nat Rev Genet *8*, 450–
1200 461. 10.1038/nrg2102.
1201 60. Matelsky, J.K., Norman-Tenazas, R., Davenport, F., Reilly, E.P., and Gray-Roncal, W. (2021).
1202 Circuit motifs and graph properties of connectome development in C. elegans (bioRxiv).
1203 61. McKay, F.M., McCoy, C.J., Crooks, B., Marks, N.J., Maule, A.G., Atkinson, L.E., and
1204 Mousley, A. (2022). In silico analyses of neuropeptide-like protein (NLP) profiles in parasitic
1205 nematodes. Int J Parasitol *52*, 77–85. 10.1016/j.ijpara.2021.07.002.
1206 62. Hobert, O. (2013). The neuronal genome of Caenorhabditis elegans. WormBook, 1–106.
1207 10.1895/wormbook.1.161.1.
1208 63. Foster, S.R., Hauser, A.S., Vedel, L., Strachan, R.T., Huang, X.-P., Gavin, A.C., Shah, S.D.,
1209 Nayak, A.P., Haugaard-Kedström, L.M., Penn, R.B., et al. (2019). Discovery of Human
1210 Signaling Systems: Pairing Peptides to G Protein-Coupled Receptors. Cell *179*, 895-908.e21.
1211 10.1016/j.cell.2019.10.010.
1212 64. Beets, I., Zels, S., Vandewyer, E., Demeulemeester, J., Caers, J., Baytemur, E., Schafer, W.R.,
1213 Vértes, P.E., Mirabeau, O., and Schoofs, L. (2022). System-wide discovery of neuropeptide-
1214 GPCR pairs in C. elegans. Preprint in bioRxiv.
1215 65. Albertson, D.G., and Thomson, J.N. The pharynx of Caenorhabditis elegans. Philos Trans R
1216 Soc Lond B Biol Sci *275*, 299–325. https://doi.org/10.1098/rstb.1976.0085.

1217 66. Witvliet, D., Mulcahy, B., Mitchell, J.K., Meirovitch, Y., Berger, D.R., Wu, Y., Liu, Y., Koh,
1218 W.X., Parvathala, R., Holmyard, D., et al. (2021). Connectomes across development reveal
1219 principles of brain maturation. Nature *596*, 257–261. 10.1038/s41586-021-03778-8.
1220 67. Moyle, M.W., Barnes, K.M., Kuchroo, M., Gonopolskiy, A., Duncan, L.H., Sengupta, T.,
1221 Shao, L., Guo, M., Santella, A., Christensen, R., et al. (2021). Structural and developmental
1222 principles of neuropil assembly in C. elegans. Nature *591*, 99–104. 10.1038/s41586-020-
1223 03169-5.
1224 68. Brittin, C.A., Cook, S.J., Hall, D.H., Emmons, S.W., and Cohen, N. (2021). A multi-scale
1225 brain map derived from whole-brain volumetric reconstructions. Nature *591*, 105–110.
1226 10.1038/s41586-021-03284-x.
1227 69. Maier, W., Adilov, B., Regenass, M., and Alcedo, J. (2010). A Neuromedin U Receptor Acts
1228 with the Sensory System to Modulate Food Type-Dependent Effects on C. elegans Lifespan.
1229 PLoS Biol *8*, e1000376. 10.1371/journal.pbio.1000376.
1230 70. Pocock, R., and Hobert, O. (2010). Hypoxia activates a latent circuit for processing gustatory
1231 information in C. elegans. Nat Neurosci *13*, 610–614. 10.1038/nn.2537.
1232 71. van Sinay, E., Mirabeau, O., Depuydt, G., van Hiel, M.B., Peymen, K., Watteyne, J., Zels, S.,
1233 Schoofs, L., and Beets, I. (2017). Evolutionarily conserved TRH neuropeptide pathway
1234 regulates growth in *Caenorhabditis elegans*. Proceedings of the National Academy of Sciences
1235 *114*. 10.1073/pnas.1617392114.
1236 72. Cook, S.J., Crouse, C.M., Yemini, E., Hall, D.H., Emmons, S.W., and Hobert, O. (2020). The
1237 connectome of the Caenorhabditis elegans pharynx. J Comp Neurol *528*, 2767–2784.
1238 10.1002/cne.24932.
1239 73. Vidal, B., Gulez, B., Cao, W.X., Leyva-Díaz, E., Reilly, M.B., Tekieli, T., and Hobert, O.
1240 (2022). The enteric nervous system of the C. elegans pharynx is specified by the Sine oculis-
1241 like homeobox gene ceh-34. Elife *11*, e76003. 10.7554/eLife.76003.
1242 74. Kaplan, H.S., Nichols, A.L.A., and Zimmer, M. (2018). Sensorimotor integration in
1243 Caenorhabditis elegans: A reappraisal towards dynamic and distributed computations.

1244 Philosophical Transactions of the Royal Society B: Biological Sciences *373*.
1245 10.1098/rstb.2017.0371.
1246 75. Pereira, L., Kratsios, P., Serrano-Saiz, E., Sheftel, H., Mayo, A.E., Hall, D.H., White, J.G.,
1247 LeBoeuf, B., Garcia, L.R., Alon, U., et al. (2015). A cellular and regulatory map of the
1248 cholinergic nervous system of C. elegans. Elife *4*, e12432. 10.7554/eLife.12432.
1249 76. Niu, L., Li, Y., Zong, P., Liu, P., Shui, Y., Chen, B., and Wang, Z.-W. (2020). Melatonin
1250 promotes sleep by activating the BK channel in C. elegans. Proc Natl Acad Sci U S A *117*,
1251 25128–25137. 10.1073/pnas.2010928117.
1252 77. Betzel, R.F., Medaglia, J.D., and Bassett, D.S. (2018). Diversity of meso-scale architecture in
1253 human and non-human connectomes. Nat Commun *9*, 346. 10.1038/s41467-017-02681-z.
1254 78. Wen, Q., Po, M.D., Hulme, E., Chen, S., Liu, X., Kwok, S.W., Gershow, M., Leifer, A.M.,
1255 Butler, V., Fang-Yen, C., et al. (2012). Proprioceptive Coupling within Motor Neurons Drives
1256 C. elegans Forward Locomotion. Neuron *76*, 750–761. 10.1016/j.neuron.2012.08.039.
1257 79. Schafer, W.R. (2015). Mechanosensory molecules and circuits in C. elegans. Pflugers Arch
1258 *467*, 39–48. 10.1007/s00424-014-1574-3.
1259 80. Fenk, L.A., and de Bono, M. (2017). Memory of recent oxygen experience switches
1260 pheromone valence in *Caenorhabditis elegans*. Proceedings of the National Academy of
1261 Sciences *114*, 4195–4200. 10.1073/pnas.1618934114.
1262 81. Guillermin, M.L., Carrillo, M.A., and Hallem, E.A. (2017). A Single Set of Interneurons
1263 Drives Opposite Behaviors in C. elegans. Current Biology *27*, 2630-2639.e6.
1264 10.1016/J.CUB.2017.07.023.
1265 82. Laurent, P., Soltesz, Z., Nelson, G.M., Chen, C., Arellano-Carbajal, F., Levy, E., and de Bono,
1266 M. (2015). Decoding a neural circuit controlling global animal state in C. Elegans. Elife *2015*.
1267 83. Busch, K.E., Laurent, P., Soltesz, Z., Murphy, R.J., Faivre, O., Hedwig, B., Thomas, M.,
1268 Smith, H.L., and de Bono, M. (2012). Tonic signaling from O2 sensors sets neural circuit
1269 activity and behavioral state. Nat Neurosci *15*, 581–591. 10.1038/nn.3061.
1270 84. Haspel, G., Deng, L., Harreguy, M.B., and Tanvir, Z. (2020). Elegantly. The Neural Control of
1271 Movement, 3–29. 10.1016/B978-0-12-816477-8.00001-6.

85. Tolstenkov, O., Van der Auwera, P., Costa, W.S., Bazhanova, O., Gemeinhardt, T.M., Bergs, A.C.F., and Gottschalk, A. (2018). Functionally asymmetric motor neurons contribute to coordinating locomotion of Caenorhabditis elegans. Elife *7*. 10.7554/ELIFE.34997.

86. Butler, V.J., Branicky, R., Yemini, E., Liewald, J.F., Gottschalk, A., Kerr, R.A., Chklovskii, D.B., and Schafer, W.R. (2015). A consistent muscle activation strategy underlies crawling and swimming in Caenorhabditis elegans. J R Soc Interface *12*. 10.1098/RSIF.2014.0963.

87. Faumont, S., Rondeau, G., Thiele, T.R., Lawton, K.J., McCormick, K.E., Sottile, M., Griesbeck, O., Heckscher, E.S., Roberts, W.M., Doe, C.Q., et al. (2011). An Image-Free Opto-Mechanical System for Creating Virtual Environments and Imaging Neuronal Activity in Freely Moving Caenorhabditis elegans. PLoS One *6*, e24666. 10.1371/journal.pone.0024666.

88. Wen, Q., Po, M., Hulme, E., Chen, S., Liu, X., Kwok, S., Gershow, M., Leifer, A., Butler, V., Fang-Yen, C., et al. (2012). Proprioceptive coupling within motor neurons drives C. elegans forward locomotion. Neuron *76*, 750–761. 10.1016/J.NEURON.2012.08.039.

89. Gao, S., Guan, S.A., Fouad, A.D., Meng, J., Kawano, T., Huang, Y.-C., Li, Y., Alcaire, S., Hung, W., Lu, Y., et al. (2018). Excitatory motor neurons are local oscillators for backward locomotion. Elife *7*. 10.7554/eLife.29915.

90. Worrell, J.C., Rumschlag, J., Betzel, R.F., Sporns, O., and Mišić, B. (2017). Optimized connectome architecture for sensory-motor integration. Netw Neurosci *1*, 415–430. 10.1162/NETN_a_00022.

91. Williams, E.A., Verasztó, C., Jasek, S., Conzelmann, M., Shahidi, R., Bauknecht, P., Mirabeau, O., and Jékely, G. (2017). Synaptic and peptidergic connectome of a neurosecretory center in the annelid brain. Elife *6*, e26349. 10.7554/eLife.26349.

92. Turek, M., Besseling, J., Spies, J.-P., König, S., and Bringmann, H. (2016). Sleep-active neuron specification and sleep induction require FLP-11 neuropeptides to systemically induce sleep. Elife *5*, e12499. 10.7554/eLife.12499.

93. Xu, Y., Zhang, L., Liu, Y., Topalidou, I., Hassinan, C., Ailion, M., Zhao, Z., Wang, T., Chen, Z., and Bai, J. (2021). Dopamine receptor DOP-1 engages a sleep pathway to modulate swimming in C. elegans. iScience *24*, 102247. 10.1016/j.isci.2021.102247.

1300 94. Priest, M.F., Freda, S.N., Badong, D., Dumrongprechachan, V., and Kozorovitskiy, Y. (2021).
1301 Peptidergic modulation of fear responses by the Edinger-Westphal nucleus (bioRxiv).
1302 95. Kim, M.W., Wang, W., Sanchez, M.I., Coukos, R., von Zastrow, M., and Ting, A.Y. (2017).
1303 Time-gated detection of protein-protein interactions with transcriptional readout. Elife *6*,
1304 e30233. 10.7554/eLife.30233.
1305 96. Kim, C.K., Cho, K.F., Kim, M.W., and Ting, A.Y. (2019). Luciferase-LOV BRET enables
1306 versatile and specific transcriptional readout of cellular protein-protein interactions. Elife *8*,
1307 e43826. 10.7554/eLife.43826.
1308 97. Smith, S.J., Smbül, U., Graybuck, L.T., Collman, F., Seshamani, S., Gala, R., Gliko, O.,
1309 Elabbady, L., Miller, J.A., Bakken, T.E., et al. (2019). Single-cell transcriptomic evidence for
1310 dense intracortical neuropeptide networks. Elife *8*, 1–35. 10.7554/eLife.47889.
1311 98. Chen, R., Wu, X., Jiang, L., and Zhang, Y. (2017). Single-Cell RNA-Seq Reveals
1312 Hypothalamic Cell Diversity. Cell Rep *18*, 3227–3241. 10.1016/J.CELREP.2017.03.004.
1313 99. Terauchi, A., Johnson-Venkatesh, B., Bullock, B., Lehtinen, M., and Umemori, H. (2016).
1314 Retrograde fibroblast growth factor 22 (FGF22) signaling regulates insulin-like growth factor
1315 2 (IGF2) expression for activity-dependent synapse stabilization in the mammalian brain. Elife
1316 *5*. 10.7554/ELIFE.12151.
1317 100. Ghosh, D.D., Sanders, T., Hong, S., McCurdy, L.Y., Chase, D.L., Cohen, N., Koelle, M.R.,
1318 and Nitabach, M.N. (2016). Neural Architecture of Hunger-Dependent Multisensory Decision
1319 Making in C. elegans. Neuron *92*, 1049–1062. 10.1016/j.neuron.2016.10.030.
1320 101. Root, C.M., Ko, K.I., Jafari, A., and Wang, J.W. (2011). Presynaptic facilitation by
1321 neuropeptide signaling mediates odor-driven food search. Cell *145*, 133–144.
1322 10.1016/j.cell.2011.02.008.
1323 102. Horowitz, L., Brandt, J., and Ringstad, N. (2019). Repression of an activity-dependent
1324 autocrine insulin signal is required for sensory neuron development in C. elegans.
1325 Development *146*. 10.1242/DEV.182873.

1326 103. Mardinly, A., Spiegel, I., Patrizi, A., Centofante, E., Bazinet, J., Tzeng, C., Mandel-Brehm, C.,
1327 Harmin, D., Adesnik, H., Fagiolini, M., et al. (2016). Sensory experience regulates cortical
1328 inhibition by inducing IGF1 in VIP neurons. Nature *531*, 371–375. 10.1038/NATURE17187.
1329 104. Choi, C., Cao, G., Tanenhaus, A., McCarthy, E., Jung, M., Schleyer, M., Shang, Y., Rosbash,
1330 M., Yin, J., and Nitabach, M. (2012). Autoreceptor control of peptide/neurotransmitter
1331 corelease from PDF neurons determines allocation of circadian activity in drosophila. Cell Rep
1332 *2*, 332–344. 10.1016/J.CELREP.2012.06.021.
1333 105. Yoshioka, J., Prince, R., Huang, H., Perkins, S., Cruz, F., MacGillivray, C., Lauffenburger, D.,
1334 and Lee, R. (2005). Cardiomyocyte hypertrophy and degradation of connexin43 through
1335 spatially restricted autocrine/paracrine heparin-binding EGF. Proc Natl Acad Sci U S A *102*,
1336 10622–10627. 10.1073/PNAS.0501198102.
1337 106. Tse, L., and Wong, Y. (2019). GPCRs in Autocrine and Paracrine Regulations. Front
1338 Endocrinol (Lausanne) *10*. 10.3389/FENDO.2019.00428.
1339 107. Yemini, E., Jucikas, T., Grundy, L.J., Brown, A.E.X., and Schafer, W.R. (2013). A database of
1340 Caenorhabditis elegans behavioral phenotypes. Nat Methods *10*, 877–879.
1341 10.1038/nmeth.2560.
1342 108. Brown, A.E.X., Yemini, E.I., Grundy, L.J., Jucikas, T., and Schafer, W.R. (2013). A
1343 dictionary of behavioral motifs reveals clusters of genes affecting Caenorhabditis elegans
1344 locomotion. Proceedings of the National Academy of Sciences *110*, 791–796.
1345 10.1073/pnas.1211447110.
1346 109. Avery, L., and Horvitz, H.R. (1989). Pharyngeal pumping continues after laser killing of the
1347 pharyngeal nervous system of C. elegans. Neuron *3*, 473–485. 10.1016/0896-6273(89)90206-
1348 7.
1349 110. Forrester, W.C., and Garriga, G. (1997). Genes necessary for C. elegans cell and growth cone
1350 migrations. Development *124*, 1831–1843. 10.1242/dev.124.9.1831.
1351 111. Yemini, E., Lin, A., Nejatbakhsh, A., Varol, E., Sun, R., Mena, G.E., Samuel, A.D.T.,
1352 Paninski, L., Venkatachalam, V., and Hobert, O. (2021). NeuroPAL: A Multicolor Atlas for

Whole-Brain Neuronal Identification in C. elegans. Cell *184*, 272-288.e11. 10.1016/j.cell.2020.12.012.

112. Hall, D.H., and Altun, Z.F. (2011). Nervous system, general description. WormAtlas: The Handbook of C.elegans Anatomy. doi:10.3908/wormatlas.1.18.

113. Rubinov, M., and Sporns, O. (2010). Complex network measures of brain connectivity: Uses and interpretations. Neuroimage *52*, 1059–1069. 10.1016/j.neuroimage.2009.10.003.

114. Fisher, R.A. (1934). Statistical methods for research workers, 5th ed. (Edinburgh).

115. Storey, J.D. (2002). A direct approach to false discovery rates. J R Stat Soc Series B Stat Methodol *64*, 479–498. 10.1111/1467-9868.00346.

116. Bounova, G., and de Weck, O. (2012). Overview of metrics and their correlation patterns for multiple-metric topology analysis on heterogeneous graph ensembles. Phys Rev E *85*, 016117. 10.1103/PhysRevE.85.016117.

117. de Domenico, M., Porter, M.A., and Arenas, A. (2015). MuxViz: a tool for multilayer analysis and visualization of networks. J Complex Netw *3*, 159–176. 10.1093/comnet/cnu038.

118. Shannon, P., Markiel, A., Ozier, O., Baliga, N.S., Wang, J.T., Ramage, D., Amin, N., Schwikowski, B., and Ideker, T. (2003). Cytoscape: A Software Environment for Integrated Models of Biomolecular Interaction Networks. Genome Res *13*, 2498–2504. 10.1101/gr.1239303.

119. Bhardwaj, A., Thapliyal, S., Dahiya, Y., and Babu, K. (2018). FLP-18 Functions through the G-Protein-Coupled Receptors NPR-1 and NPR-4 to Modulate Reversal Length in Caenorhabditis elegans. The Journal of Neuroscience *38*, 4641–4654. 10.1523/JNEUROSCI.1955-17.2018.

120. Lindemans, M., Liu, F., Janssen, T., Husson, S.J., Mertens, I., Gäde, G., and Schoofs, L. (2009). Adipokinetic hormone signaling through the gonadotropin-releasing hormone receptor modulates egg-laying in Caenorhabditis elegans. Proceedings of the National Academy of Sciences *106*, 1642–1647. 10.1073/pnas.0809881106.

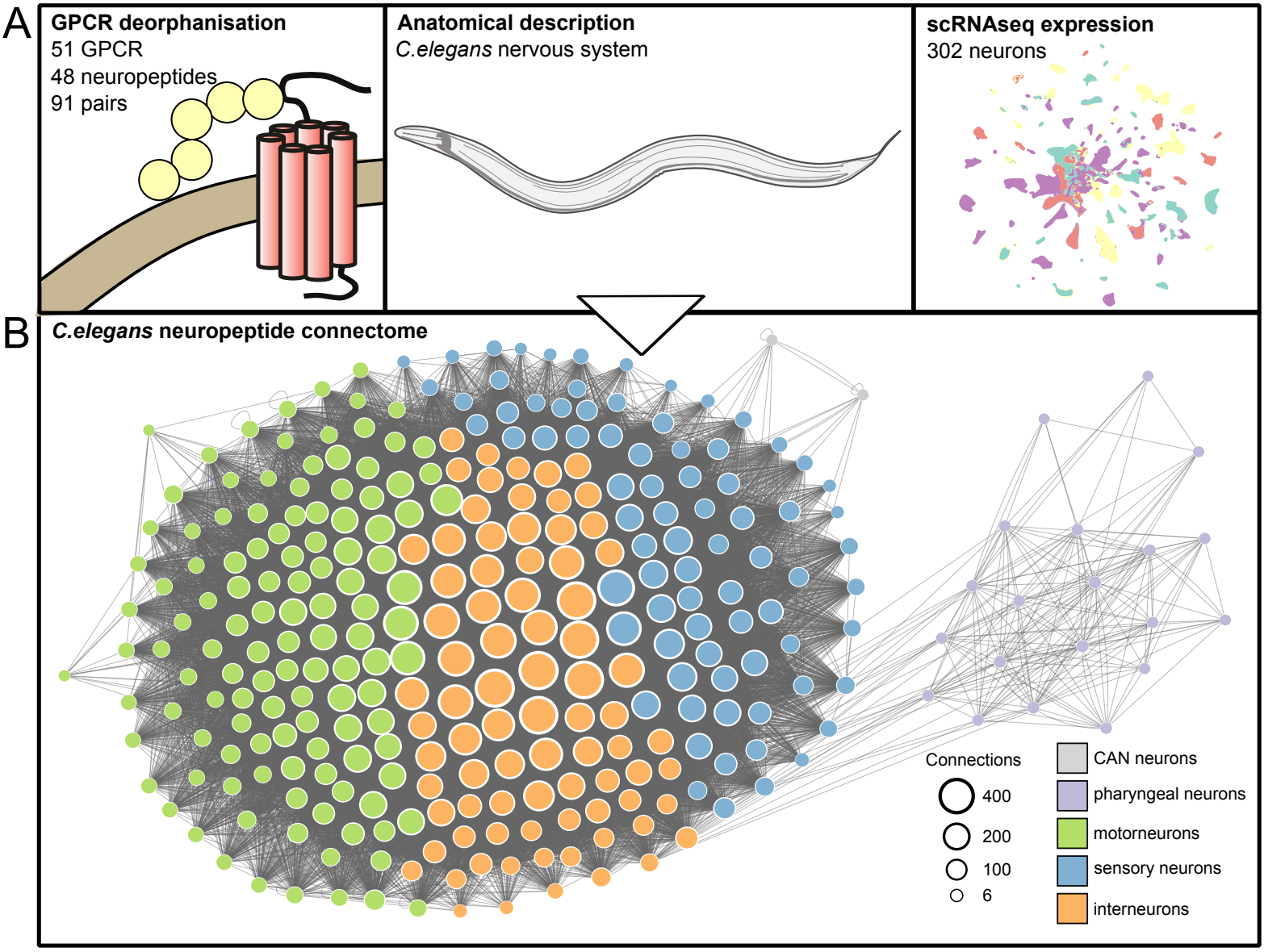
A
GPCR deorphanisation
51 GPCR
48 neuropeptides
91 pairs
Anatomical description
C.elegans nervous system
scRNAseq expression
302 neurons
B
C.elegans neuropeptide connectome
Connections
400
200
100
6
CAN neurons
pharyngeal neurons
motorneurons
sensory neurons
interneurons

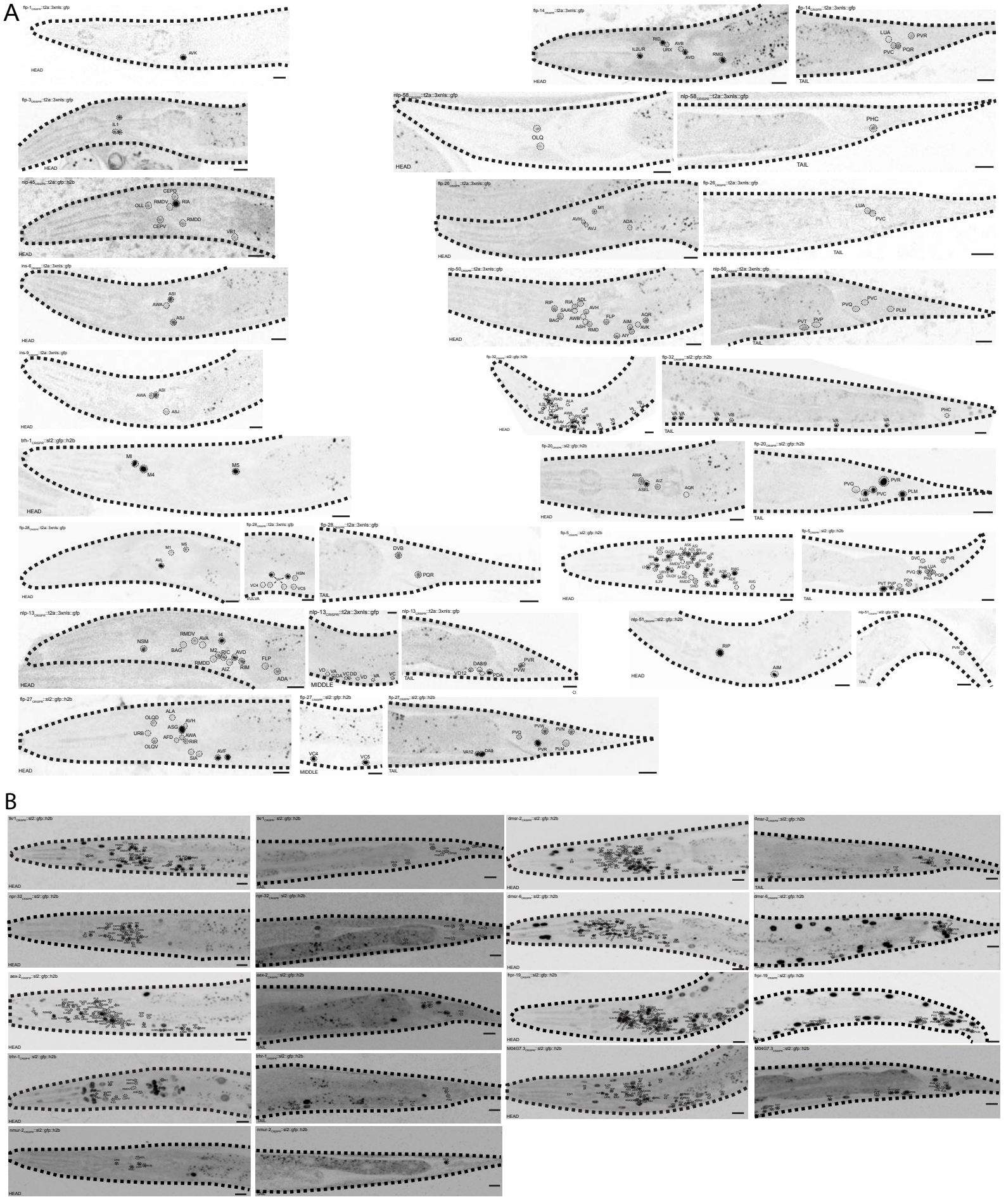
A
flp-1CRISPR::t2a::3xnls::gfp
AVK
HEAD
flp-14CRISPR::t2a::3xnls::gfp
RID
AVB
IL2L/R
URX
AVD
RMG
HEAD
flp-14CRISPR::t2a::3xnls::gfp
LUA
PVR
PVC
PQR
TAIL
flp-3CRISPR::t2a::3xnls::gfp
IL1
HEAD
nlp-58CRISPR::t2a::3xnls::gfp
OLQ
HEAD
nlp-58CRISPR::t2a::3xnls::gfp
PHC
TAIL
nlp-45CRISPR::t2a::gfp::h2b
CEPD
OLL
RMDV
RIA
RMDD
CEPV
VB1
HEAD
flp-26CRISPR::t2a::3xnls::gfp
M1
AVH
AVJ
ADA
HEAD
flp-26CRISPR::t2a::3xnls::gfp
LUA
PVC
TAIL
ins-6CRISPR::t2a::3xnls::gfp
ASI
AWA
ASJ
HEAD
nlp-50CRISPR::t2a::3xnls::gfp
RIP
RIA
ADL
SAAD
AVH
BAG
AWB
FLP
AQR
ASH
RMD
AIM
AVK
AIY
HEAD
nlp-50CRISPR::t2a::3xnls::gfp
PVQ
PVC
PLM
PVT
PVP
TAIL
ins-9CRISPR::t2a::3xnls::gfp
AWA
ASI
ASJ
HEAD
flp-32CRISPR::sl2::gfp::h2b
HEAD
flp-32CRISPR::sl2::gfp::h2b
VA
VB
PHC
TAIL
trh-1CRISPR::sl2::gfp::h2b
MI
M4
M5
HEAD
flp-20CRISPR::sl2::gfp::h2b
AWA
AIZ
ASEL
AQR
HEAD
flp-20CRISPR::sl2::gfp::h2b
PVQ
PVR
LUA
PVC
PLM
TAIL
flp-28CRISPR::t2a::3xnls::gfp
M1
M5
AVL
HEAD
flp-28CRISPR::t2a::3xnls::gfp
HSN
VC4
VC5
VULVA
flp-28CRISPR::t2a::3xnls::gfp
DVB
PQR
TAIL
flp-5CRISPR::sl2::gfp::h2b
HEAD
flp-5CRISPR::sl2::gfp::h2b
DVC
PVR
LUA
PVQ
PHA
PVT
PVP
PDA
TAIL
nlp-13CRISPR::t2a::3xnls::gfp
NSM
RMDV
AVA
I4
BAG
M2
RIC
AVD
RMDD
FLP
AIZ
RIM
ADA
HEAD
nlp-13CRISPR::t2a::3xnls::gfp
VD
VA
VCDD
VD
VA
VC
MIDDLE
nlp-13CRISPR::t2a::3xnls::gfp
PVR
DA8/9
VD12
PDA
PVW
TAIL
nlp-51CRISPR::sl2::gfp::h2b
RIP
AIM
HEAD
nlp-51CRISPR::sl2::gfp::h2b
PVR
TAIL
flp-27CRISPR::sl2::gfp::h2b
ALA
OLQD
AVH
ASG
URB
AFD
AWA
RIR
OLQV
SIA
AVF
HEAD
flp-27CRISPR::sl2::gfp::h2b
VC4
VC5
MIDDLE
flp-27CRISPR::sl2::gfp::h2b
PVQ
PVN
PVR
PLM
VA12
DA9
TAIL
B
tkr1CRISPR::sl2::gfp::h2b
HEAD
tkr1CRISPR::sl2::gfp::h2b
TAIL
dmsr-2CRISPR::sl2::gfp::h2b
HEAD
dmsr-2CRISPR::sl2::gfp::h2b
TAIL
npr-32CRISPR::sl2::gfp::h2b
HEAD
npr-32CRISPR::sl2::gfp::h2b
TAIL
dmsr-6CRISPR::sl2::gfp::h2b
HEAD
dmsr-6CRISPR::sl2::gfp::h2b
TAIL
aex-2CRISPR::sl2::gfp::h2b
HEAD
aex-2CRISPR::sl2::gfp::h2b
TAIL
frpr-19CRISPR::sl2::gfp::h2b
HEAD
frpr-19CRISPR::sl2::gfp::h2b
TAIL
trhr-1CRISPR::sl2::gfp::h2b
HEAD
trhr-1CRISPR::sl2::gfp::h2b
TAIL
M04G7.3CRISPR::sl2::gfp::h2b
HEAD
M04G7.3CRISPR::sl2::gfp::h2b
TAIL
nmur-2CRISPR::sl2::gfp::h2b
HEAD
nmur-2CRISPR::sl2::gfp::h2b
TAIL

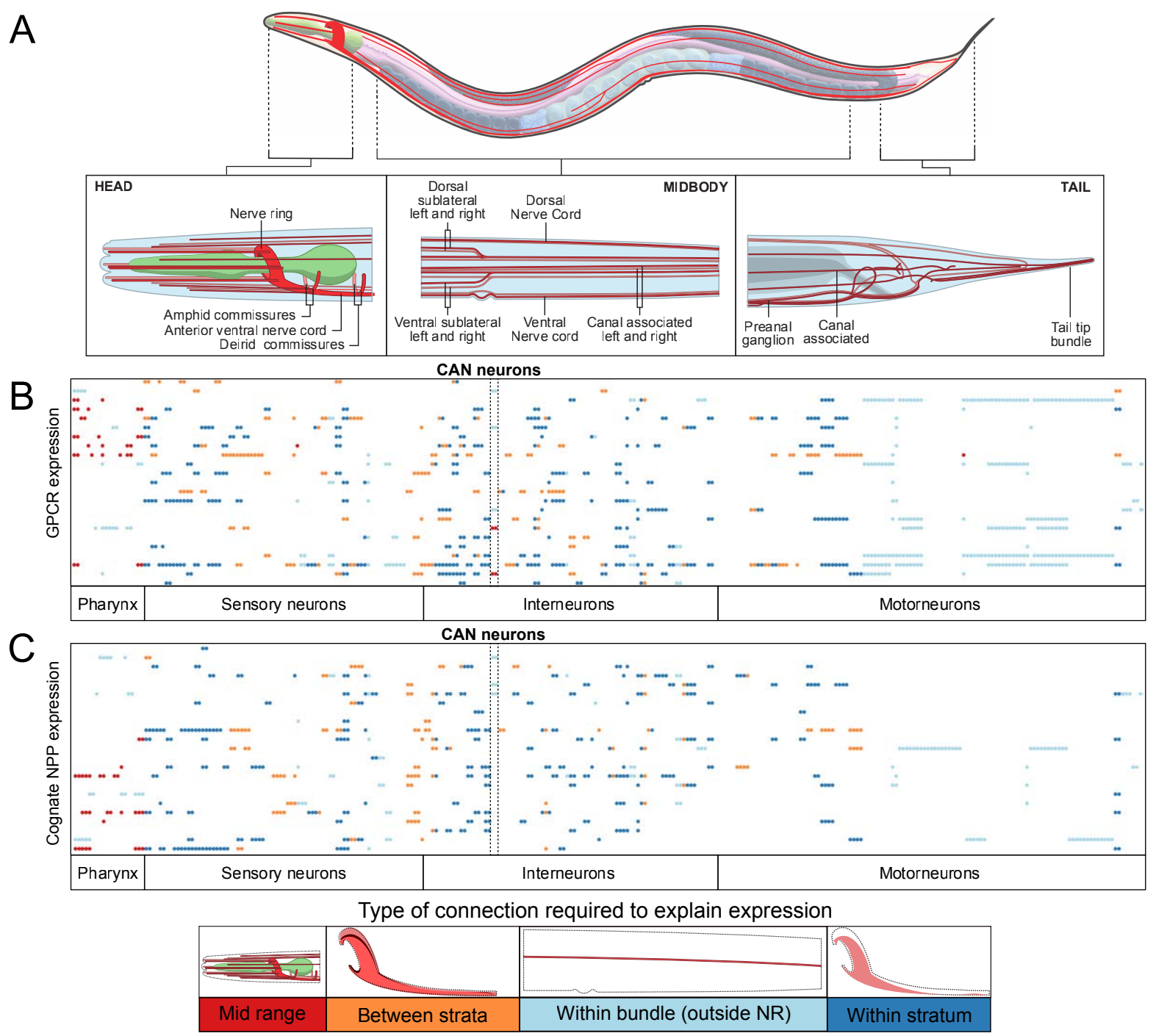
A
HEAD
Nerve ring
Amphid commissures
Anterior ventral nerve cord
Deirid commissures
MIDBODY
Dorsal sublateral left and right
Dorsal Nerve Cord
Ventral sublateral left and right
Ventral Nerve cord
Canal associated left and right
TAIL
Preanal ganglion
Canal associated
Tail tip bundle
B
CAN neurons
GPCR expression
Pharynx
Sensory neurons
Interneurons
Motorneurons
C
CAN neurons
Cognate NPP expression
Pharynx
Sensory neurons
Interneurons
Motorneurons
Type of connection required to explain expression
Mid range
Between strata
Within bundle (outside NR)
Within stratum

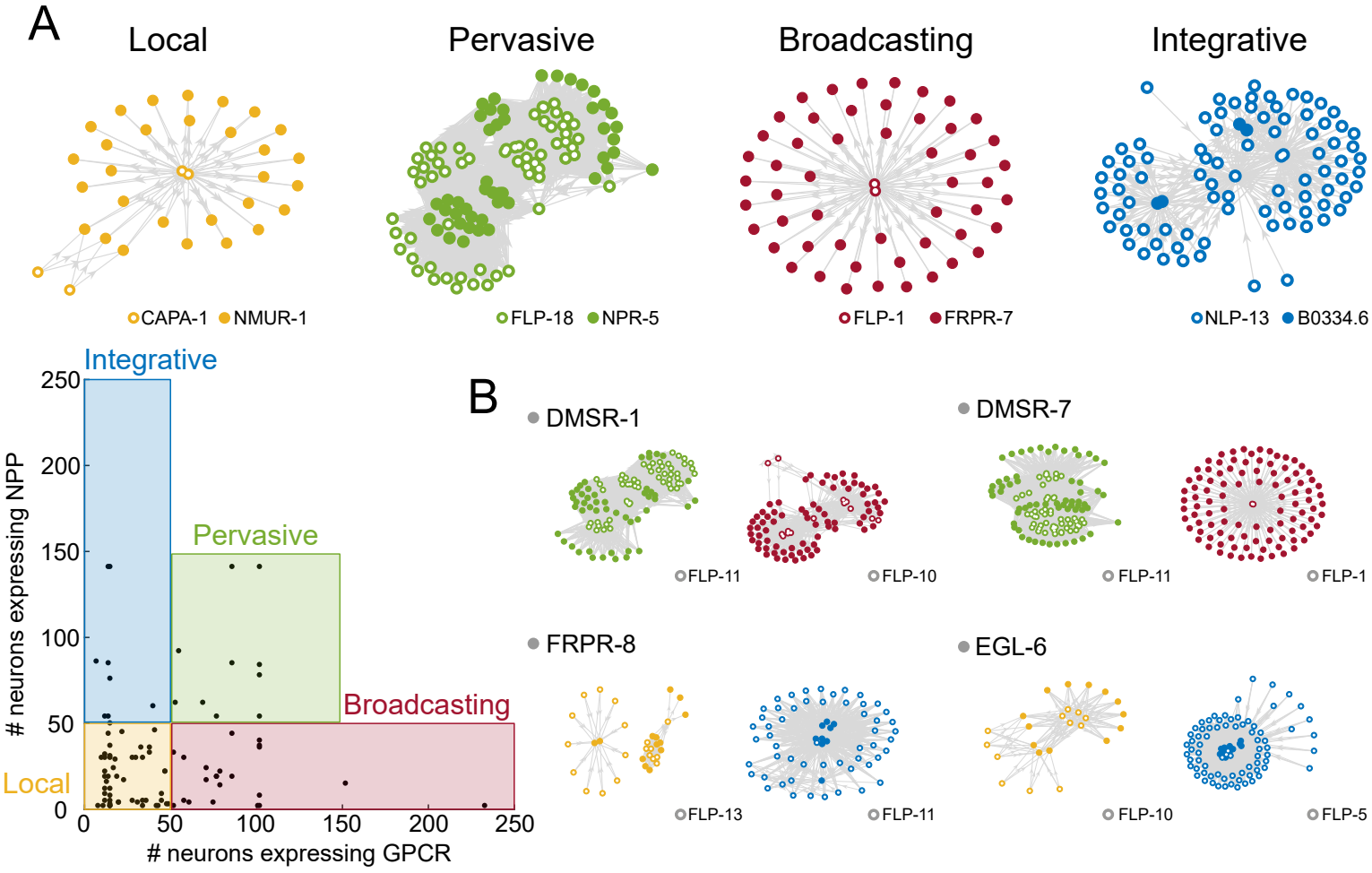
A
Local
Pervasive
Broadcasting
Integrative
CAPA-1
NMUR-1
FLP-18
NPR-5
FLP-1
FRPR-7
NLP-13
B0334.6
Integrative
Pervasive
Broadcasting
Local
neurons expressing NPP
neurons expressing GPCR
0
50
100
150
200
250
B
DMSR-1
FLP-11
FLP-10
DMSR-7
FLP-11
FLP-1
FRPR-8
FLP-13
FLP-11
EGL-6
FLP-10
FLP-5

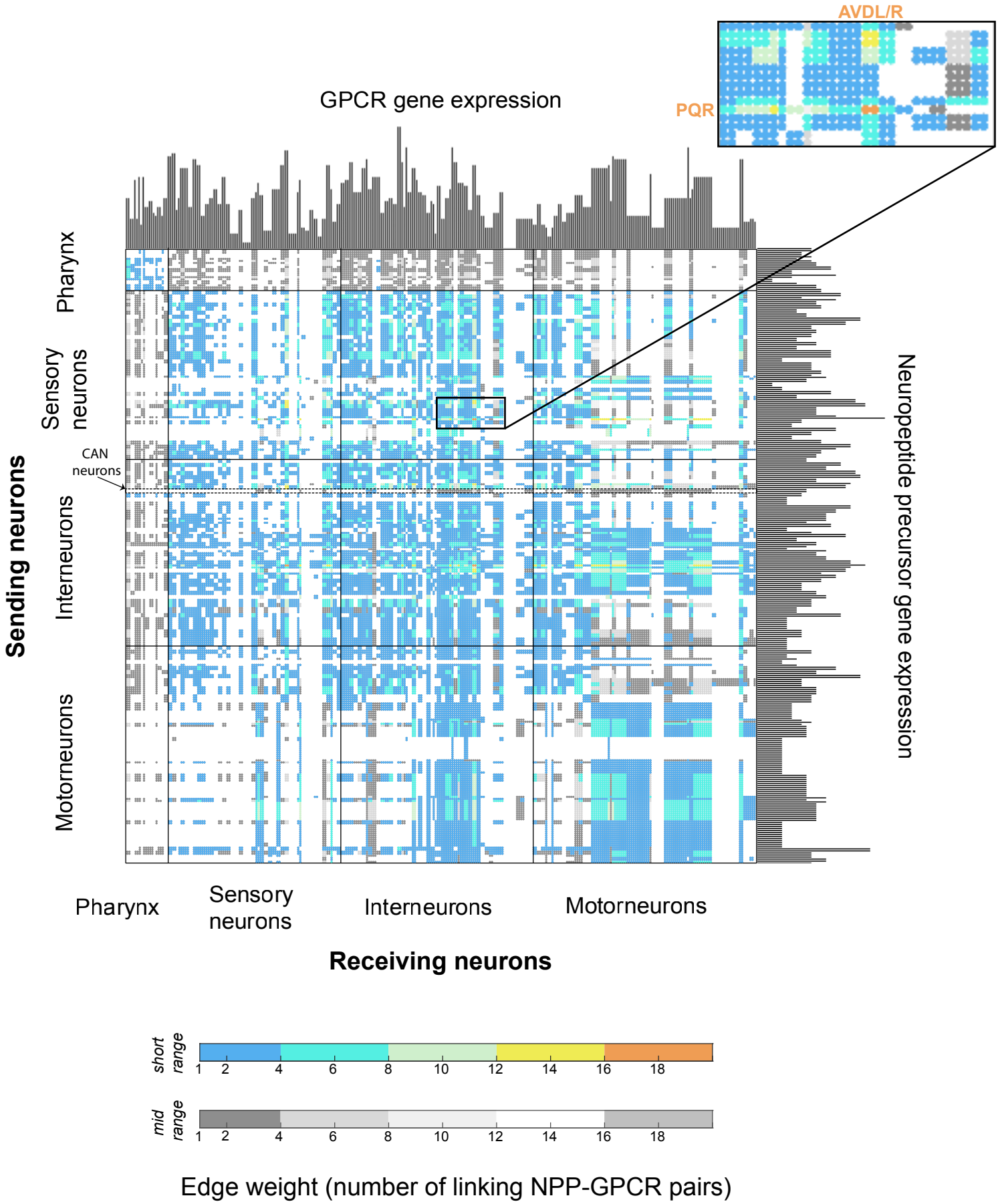
AVDL/R
PQR
GPCR gene expression
Pharynx
Sensory neurons
CAN neurons
Interneurons
Motorneurons
Sending neurons
Neuropeptide precursor gene expression
Pharynx
Sensory neurons
Interneurons
Motorneurons
Receiving neurons
short range
mid range
1 2 4 6 8 10 12 14 16 18
Edge weight (number of linking NPP-GPCR pairs)

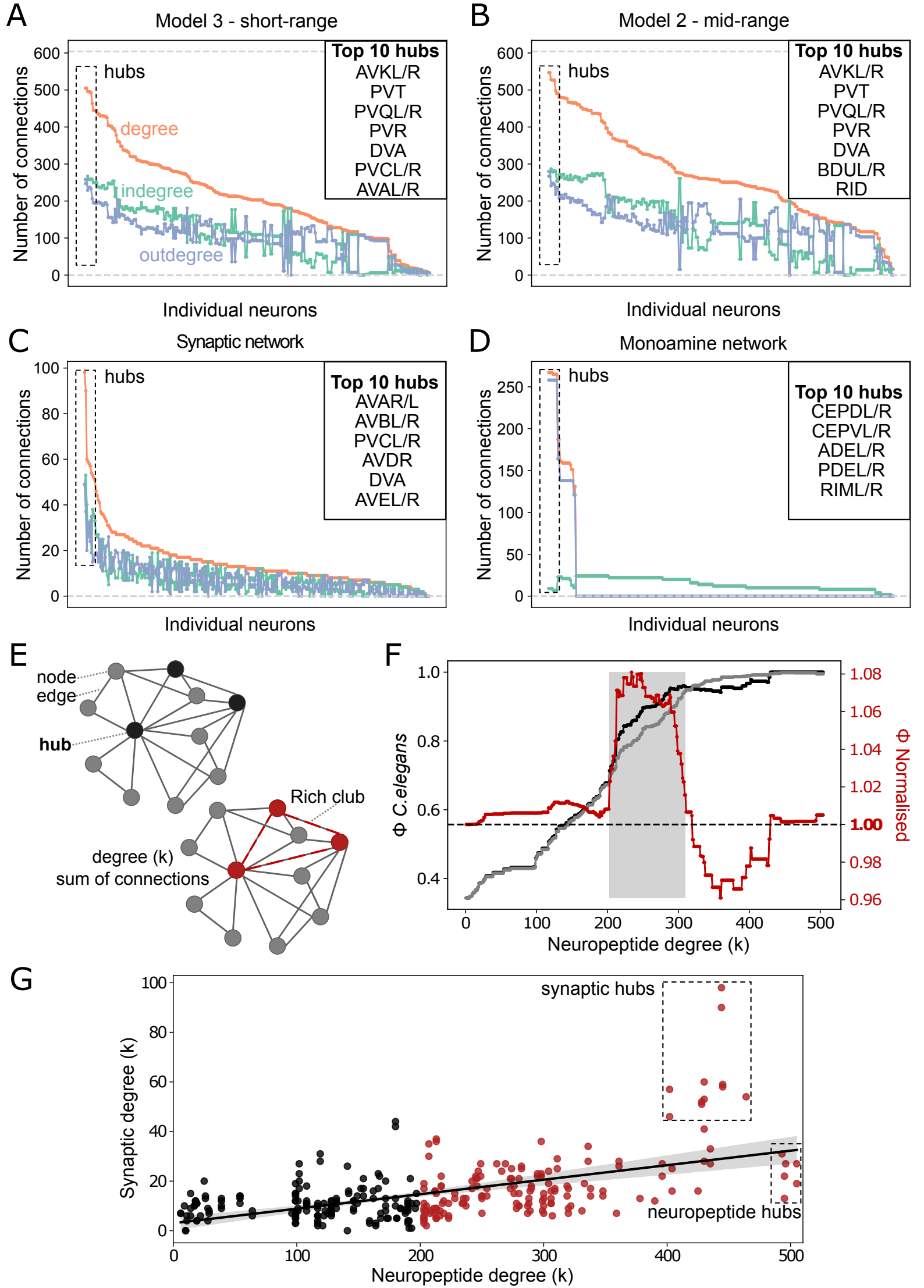
A
Model 3 - short-range
Number of connections
hubs
degree
indegree
outdegree
Top 10 hubs
AVKL/R
PVT
PVQL/R
PVR
DVA
PVCL/R
AVAL/R
Individual neurons
B
Model 2 - mid-range
Number of connections
hubs
Top 10 hubs
AVKL/R
PVT
PVQL/R
PVR
DVA
BDUL/R
RID
Individual neurons
C
Synaptic network
Number of connections
hubs
Top 10 hubs
AVAR/L
AVBL/R
PVCL/R
AVDR
DVA
AVEL/R
Individual neurons
D
Monoamine network
Number of connections
hubs
Top 10 hubs
CEPDL/R
CEPVL/R
ADEL/R
PDEL/R
RIML/R
Individual neurons
E
node
edge
hub
Rich club
degree (k)
sum of connections
F
Φ C.elegans
Φ Normalised
Neuropeptide degree (k)
G
Synaptic degree (k)
synaptic hubs
neuropeptide hubs
Neuropeptide degree (k)

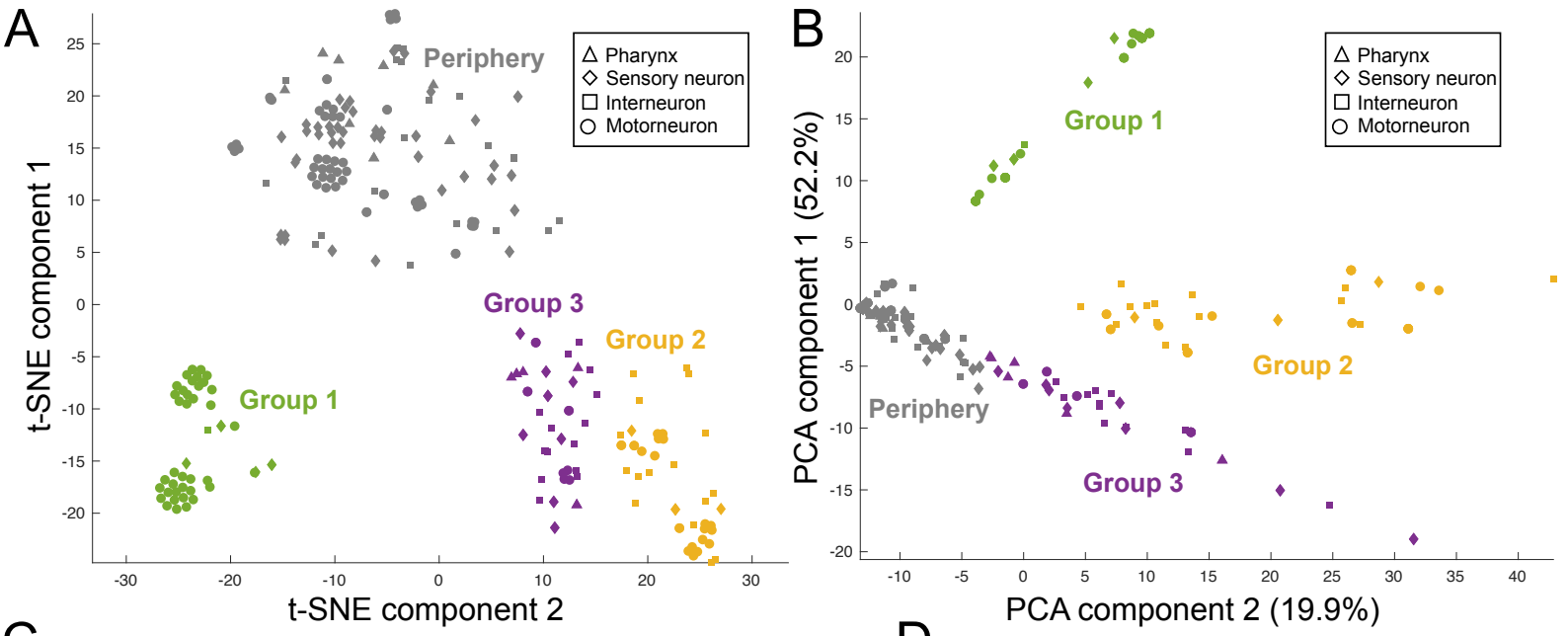

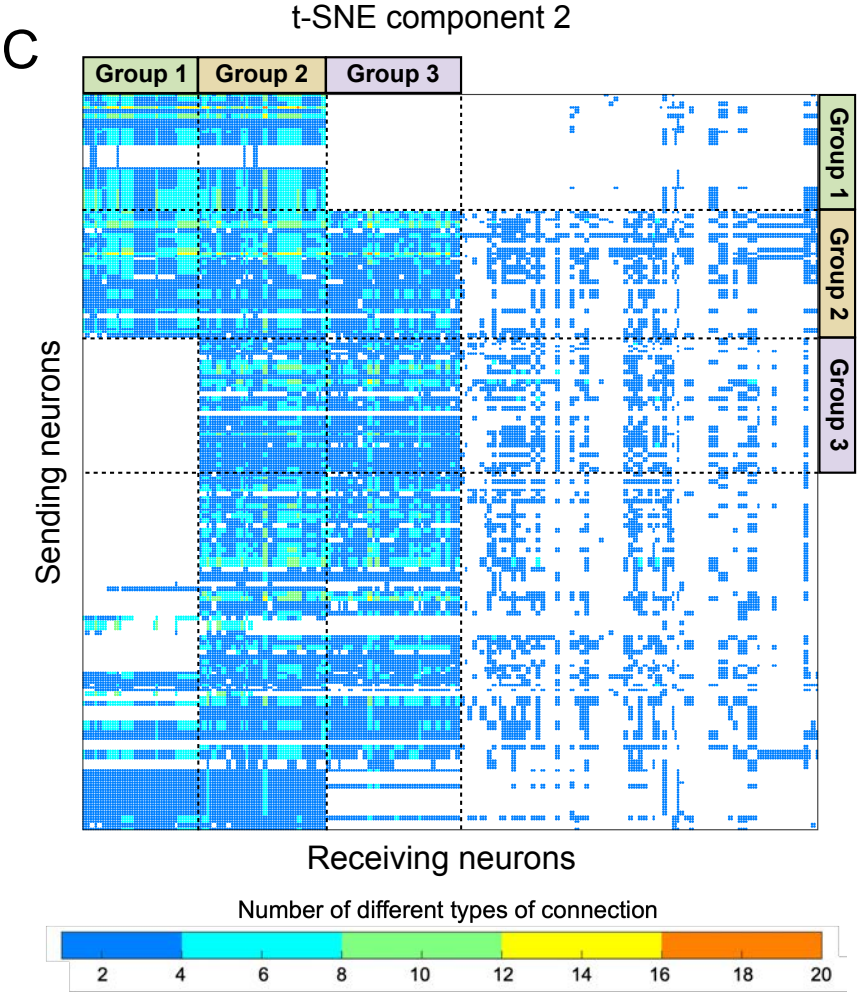

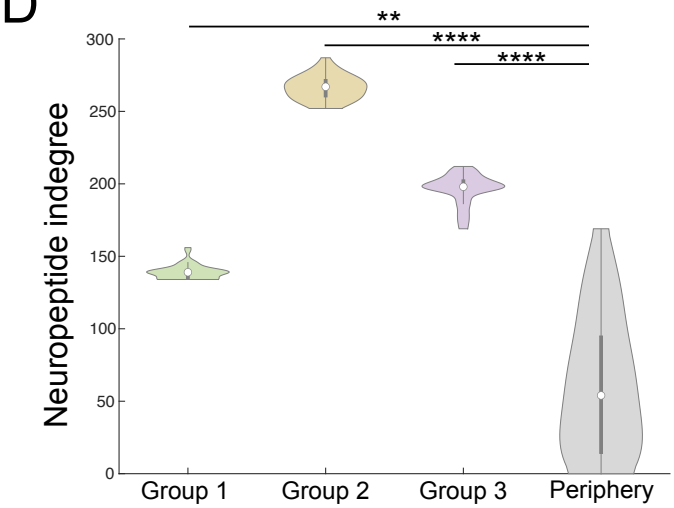

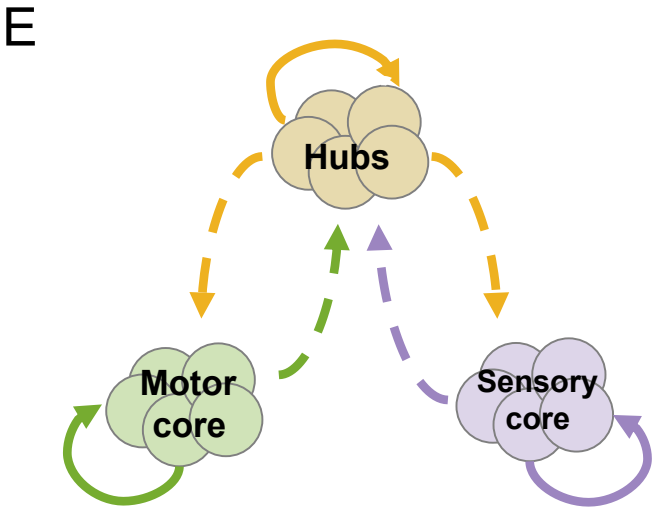

	Group 1	Group 2	Group 3
Driving neurons	DA09	PVQL/R	RIR
	VA12	PVNL/R	I5
	VC06	AVAL/R	I4
	DA08	PVR	RICL/R

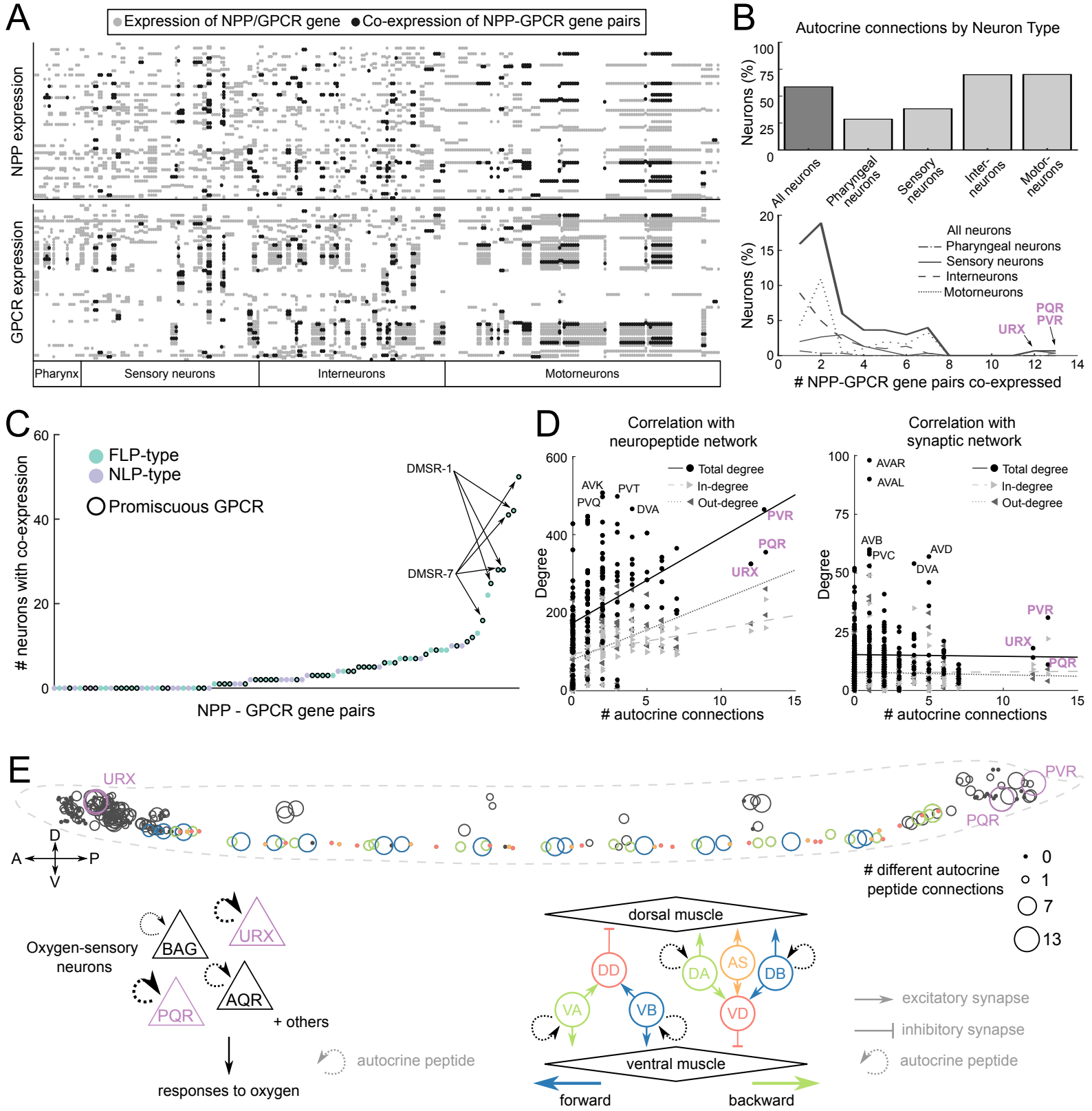
A
Expression of NPP/GPCR gene
Co-expression of NPP-GPCR gene pairs
NPP expression
GPCR expression
Pharynx
Sensory neurons
Interneurons
Motorneurons
B
Autocrine connections by Neuron Type
Neurons (%)
All neurons
Pharyngeal neurons
Sensory neurons
Inter-neurons
Motor-neurons
Neurons (%)
All neurons
Pharyngeal neurons
Sensory neurons
Interneurons
Motorneurons
PQR
PVR
URX
NPP-GPCR gene pairs co-expressed
C
FLP-type
NLP-type
Promiscuous GPCR
DMSR-1
DMSR-7
neurons with co-expression
NPP - GPCR gene pairs
D
Correlation with neuropeptide network
Total degree
In-degree
Out-degree
AVK
PVQ
PVT
DVA
PVR
PQR
URX
Degree
autocrine connections
Correlation with synaptic network
AVAR
AVAL
AVB
PVC
AVD
DVA
PVR
URX
PQR
Degree
autocrine connections
E
URX
PVR
PQR
D
A
P
V
different autocrine peptide connections
0
1
7
13
Oxygen-sensory neurons
BAG
URX
PQR
AQR
+ others
responses to oxygen
autocrine peptide
dorsal muscle
DD
DA
AS
DB
VA
VB
VD
ventral muscle
forward
backward
excitatory synapse
inhibitory synapse
autocrine peptide

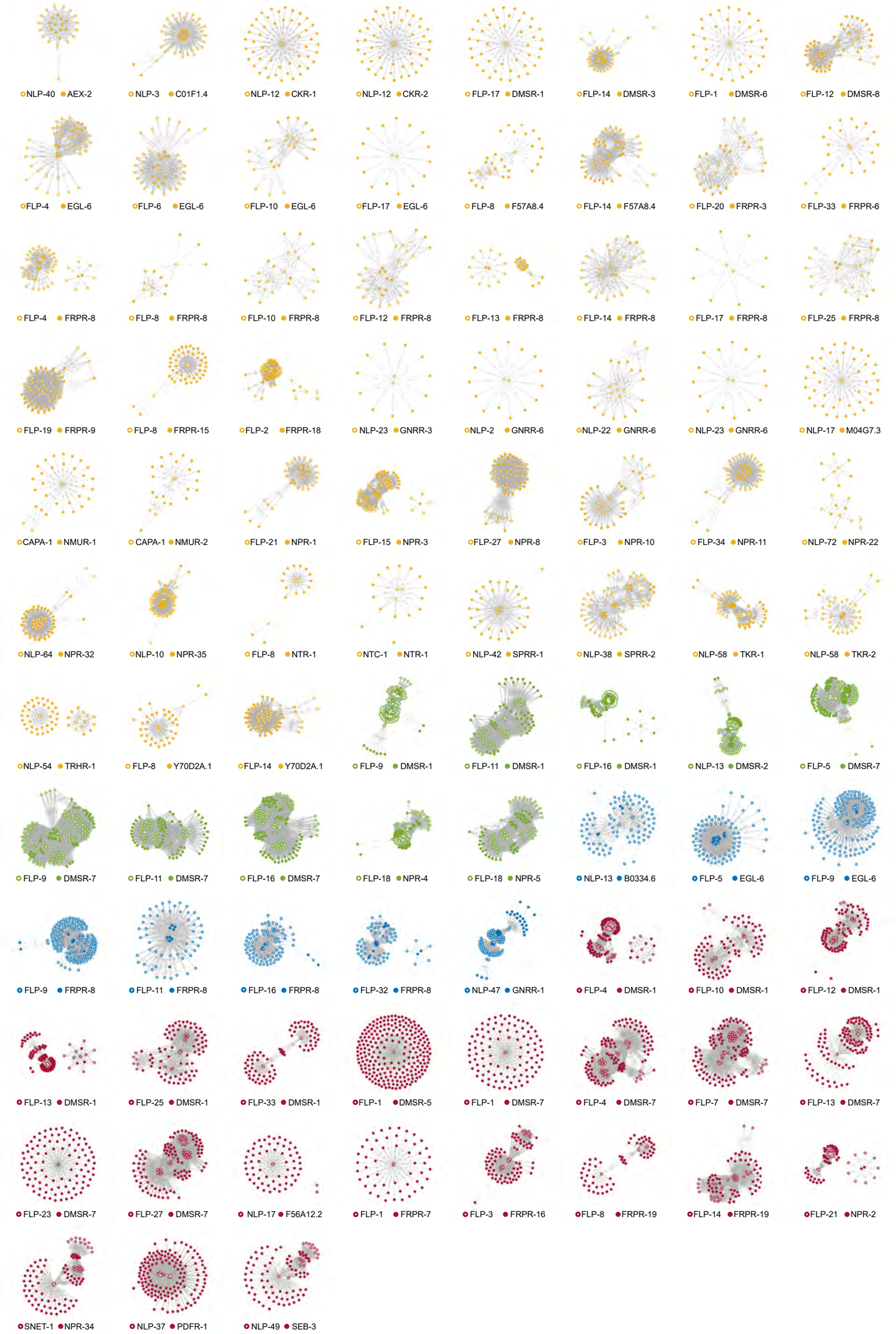
NLP-40 AEX-2
NLP-3 C01F1.4
NLP-12 CKR-1
NLP-12 CKR-2
FLP-17 DMSR-1
FLP-14 DMSR-3
FLP-1 DMSR-6
FLP-12 DMSR-8
FLP-4 EGL-6
FLP-6 EGL-6
FLP-10 EGL-6
FLP-17 EGL-6
FLP-8 F57A8.4
FLP-14 F57A8.4
FLP-20 FRPR-3
FLP-33 FRPR-6
FLP-4 FRPR-8
FLP-8 FRPR-8
FLP-10 FRPR-8
FLP-12 FRPR-8
FLP-13 FRPR-8
FLP-14 FRPR-8
FLP-17 FRPR-8
FLP-25 FRPR-8
FLP-19 FRPR-9
FLP-8 FRPR-15
FLP-2 FRPR-18
NLP-23 GNRR-3
NLP-2 GNRR-6
NLP-22 GNRR-6
NLP-23 GNRR-6
NLP-17 M04G7.3
CAPA-1 NMUR-1
CAPA-1 NMUR-2
FLP-21 NPR-1
FLP-15 NPR-3
FLP-27 NPR-8
FLP-3 NPR-10
FLP-34 NPR-11
NLP-72 NPR-22
NLP-64 NPR-32
NLP-10 NPR-35
FLP-8 NTR-1
NTC-1 NTR-1
NLP-42 SPRR-1
NLP-38 SPRR-2
NLP-58 TKR-1
NLP-58 TKR-2
NLP-54 TRHR-1
FLP-8 Y70D2A.1
FLP-14 Y70D2A.1
FLP-9 DMSR-1
FLP-11 DMSR-1
FLP-16 DMSR-1
NLP-13 DMSR-2
FLP-5 DMSR-7
FLP-9 DMSR-7
FLP-11 DMSR-7
FLP-16 DMSR-7
FLP-18 NPR-4
FLP-18 NPR-5
NLP-13 B0334.6
FLP-5 EGL-6
FLP-9 EGL-6
FLP-9 FRPR-8
FLP-11 FRPR-8
FLP-16 FRPR-8
FLP-32 FRPR-8
NLP-47 GNRR-1
FLP-4 DMSR-1
FLP-10 DMSR-1
FLP-12 DMSR-1
FLP-13 DMSR-1
FLP-25 DMSR-1
FLP-33 DMSR-1
FLP-1 DMSR-5
FLP-1 DMSR-7
FLP-4 DMSR-7
FLP-7 DMSR-7
FLP-13 DMSR-7
FLP-23 DMSR-7
FLP-27 DMSR-7
NLP-17 F56A12.2
FLP-1 FRPR-7
FLP-3 FRPR-16
FLP-8 FRPR-19
FLP-14 FRPR-19
FLP-21 NPR-2
SNET-1 NPR-34
NLP-37 PDFR-1
NLP-49 SEB-3

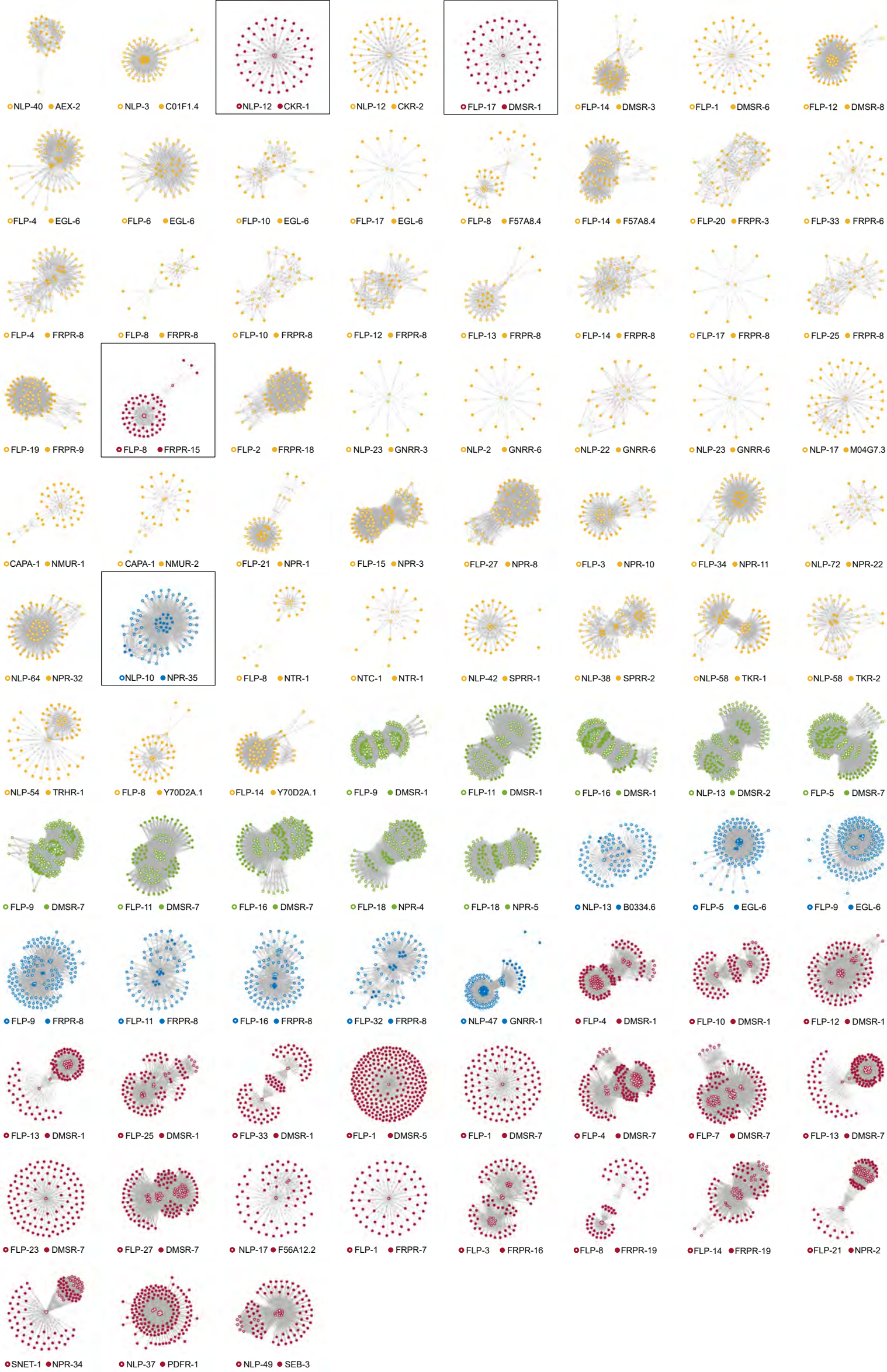
NLP-40 AEX-2
NLP-3 C01F1.4
NLP-12 CKR-1
NLP-12 CKR-2
FLP-17 DMSR-1
FLP-14 DMSR-3
FLP-1 DMSR-6
FLP-12 DMSR-8
FLP-4 EGL-6
FLP-6 EGL-6
FLP-10 EGL-6
FLP-17 EGL-6
FLP-8 F57A8.4
FLP-14 F57A8.4
FLP-20 FRPR-3
FLP-33 FRPR-6
FLP-4 FRPR-8
FLP-8 FRPR-8
FLP-10 FRPR-8
FLP-12 FRPR-8
FLP-13 FRPR-8
FLP-14 FRPR-8
FLP-17 FRPR-8
FLP-25 FRPR-8
FLP-19 FRPR-9
FLP-8 FRPR-15
FLP-2 FRPR-18
NLP-23 GNRR-3
NLP-2 GNRR-6
NLP-22 GNRR-6
NLP-23 GNRR-6
NLP-17 M04G7.3
CAPA-1 NMUR-1
CAPA-1 NMUR-2
FLP-21 NPR-1
FLP-15 NPR-3
FLP-27 NPR-8
FLP-3 NPR-10
FLP-34 NPR-11
NLP-72 NPR-22
NLP-64 NPR-32
NLP-10 NPR-35
FLP-8 NTR-1
NTC-1 NTR-1
NLP-42 SPRR-1
NLP-38 SPRR-2
NLP-58 TKR-1
NLP-58 TKR-2
NLP-54 TRHR-1
FLP-8 Y70D2A.1
FLP-14 Y70D2A.1
FLP-9 DMSR-1
FLP-11 DMSR-1
FLP-16 DMSR-1
NLP-13 DMSR-2
FLP-5 DMSR-7
FLP-9 DMSR-7
FLP-11 DMSR-7
FLP-16 DMSR-7
FLP-18 NPR-4
FLP-18 NPR-5
NLP-13 B0334.6
FLP-5 EGL-6
FLP-9 EGL-6
FLP-9 FRPR-8
FLP-11 FRPR-8
FLP-16 FRPR-8
FLP-32 FRPR-8
NLP-47 GNRR-1
FLP-4 DMSR-1
FLP-10 DMSR-1
FLP-12 DMSR-1
FLP-13 DMSR-1
FLP-25 DMSR-1
FLP-33 DMSR-1
FLP-1 DMSR-5
FLP-1 DMSR-7
FLP-4 DMSR-7
FLP-7 DMSR-7
FLP-13 DMSR-7
FLP-23 DMSR-7
FLP-27 DMSR-7
NLP-17 F56A12.2
FLP-1 FRPR-7
FLP-3 FRPR-16
FLP-8 FRPR-19
FLP-14 FRPR-19
FLP-21 NPR-2
SNET-1 NPR-34
NLP-37 PDFR-1
NLP-49 SEB-3

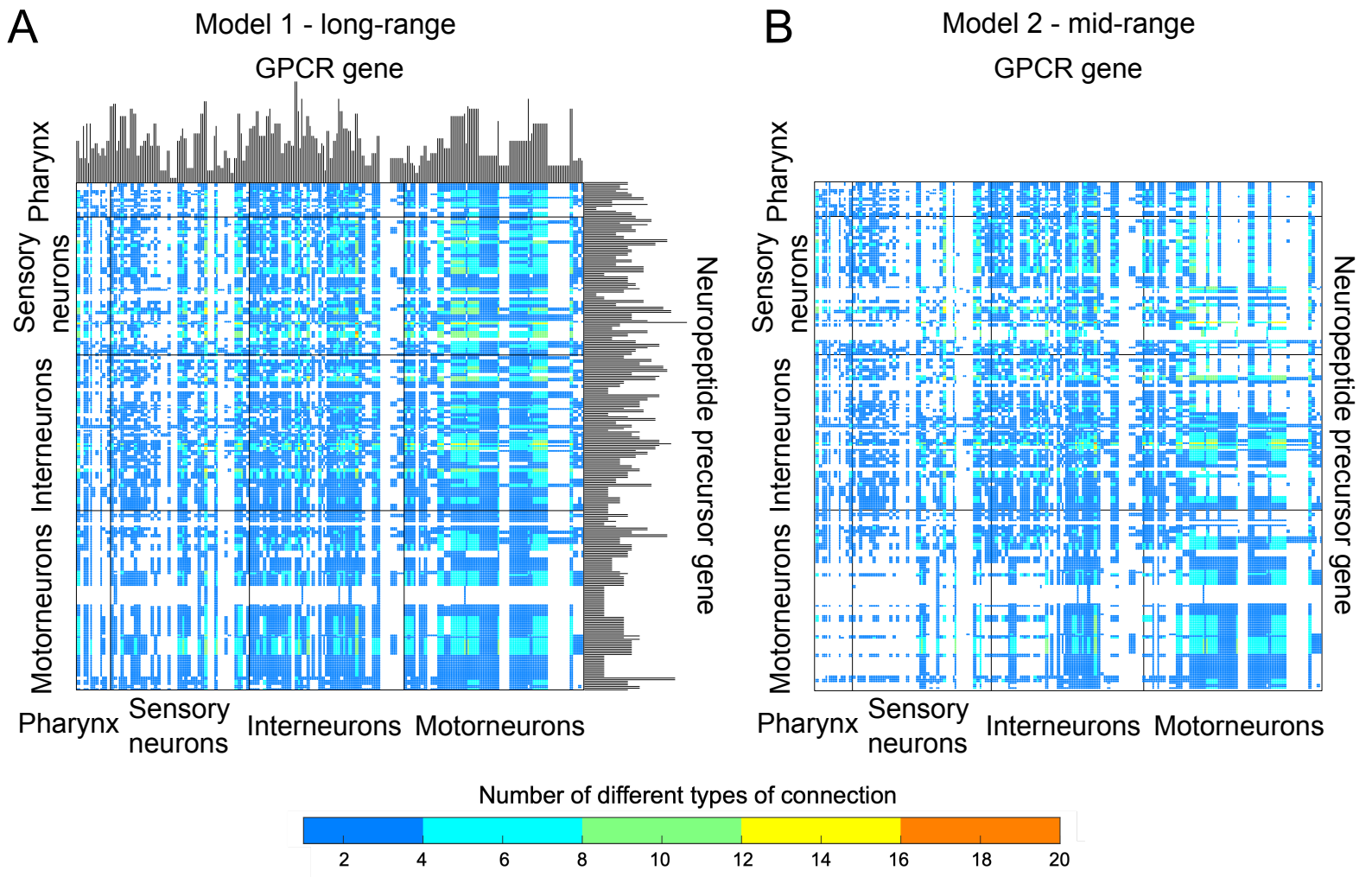
A
Model 1 - long-range
GPCR gene
Pharynx
Sensory neurons
Interneurons
Motorneurons
Neuropeptide precursor gene
Pharynx
Sensory neurons
Interneurons
Motorneurons
B
Model 2 - mid-range
GPCR gene
Pharynx
Sensory neurons
Interneurons
Motorneurons
Neuropeptide precursor gene
Pharynx
Sensory neurons
Interneurons
Motorneurons
Number of different types of connection
2
4
6
8
10
12
14
16
18
20

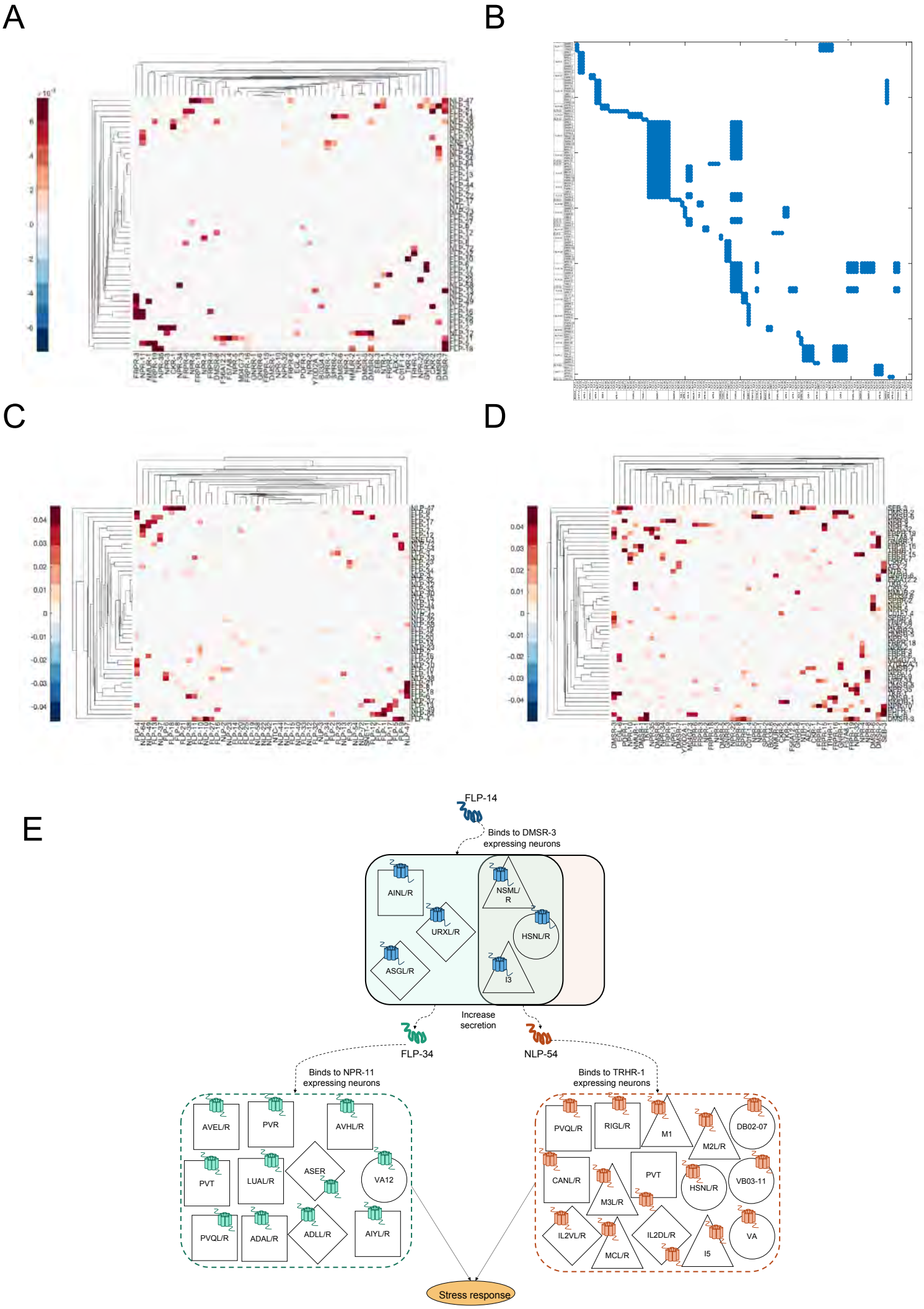
A
B
C
D
E
FLP-14
Binds to DMSR-3 expressing neurons
AINL/R
URXL/R
ASGL/R
NSML/R
HSNL/R
I3
Increase secretion
FLP-34
NLP-54
Binds to NPR-11 expressing neurons
AVEL/R
PVR
AVHL/R
PVT
LUAL/R
ASER
VA12
PVQL/R
ADAL/R
ADLL/R
AIYL/R
Binds to TRHR-1 expressing neurons
PVQL/R
RIGL/R
M1
M2L/R
DB02-07
CANL/R
PVT
HSNL/R
VB03-11
M3L/R
IL2VL/R
IL2DL/R
VA
MCL/R
I5
Stress response

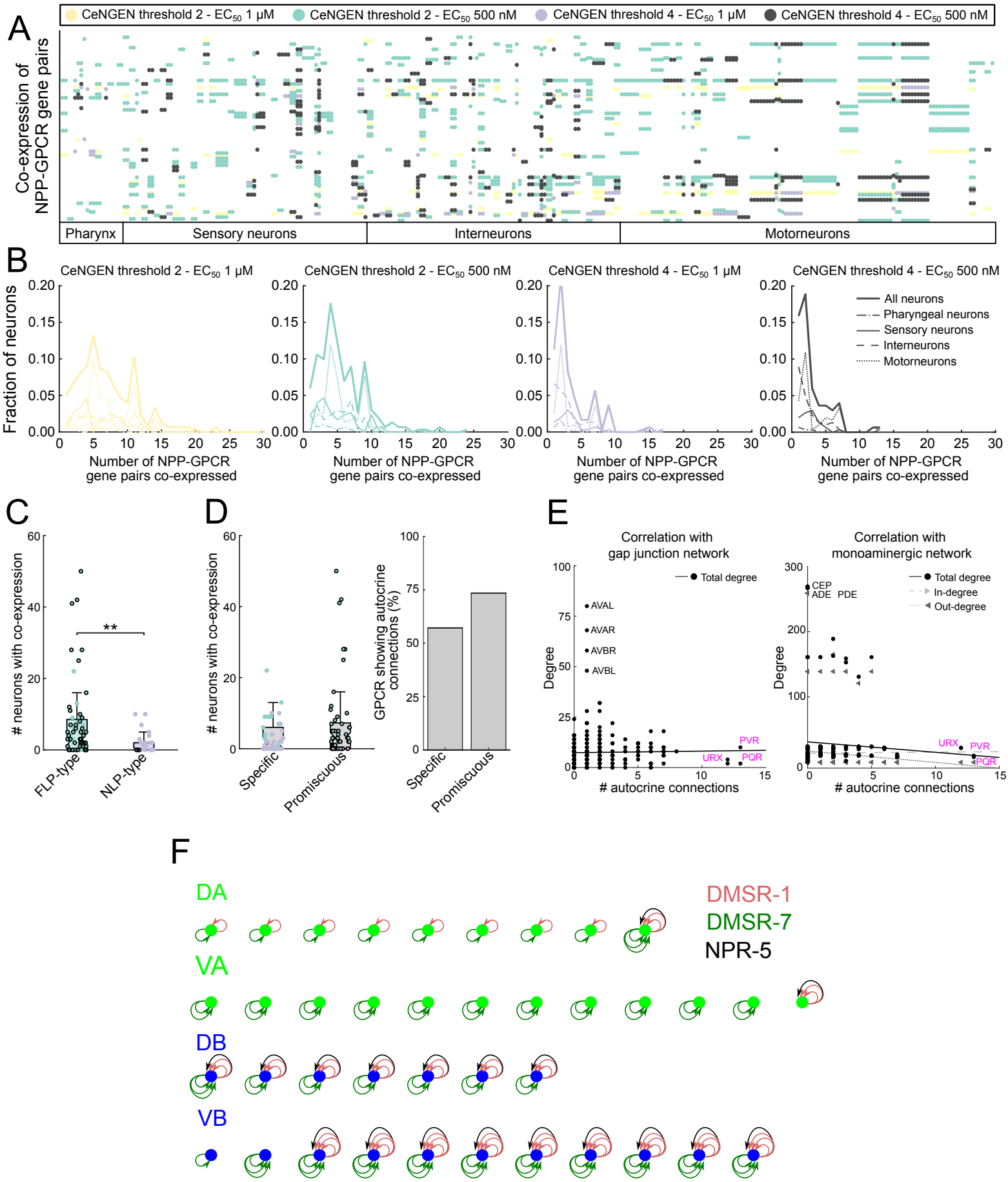
A
CeNGEN threshold 2 - EC50 1 μM
CeNGEN threshold 2 - EC50 500 nM
CeNGEN threshold 4 - EC50 1 μM
CeNGEN threshold 4 - EC50 500 nM
Co-expression of NPP-GPCR gene pairs
Pharynx
Sensory neurons
Interneurons
Motorneurons
B
Fraction of neurons
Number of NPP-GPCR gene pairs co-expressed
All neurons
Pharyngeal neurons
Sensory neurons
Interneurons
Motorneurons
C
neurons with co-expression
FLP-type
NLP-type
D
neurons with co-expression
Specific
Promiscuous
GPCR showing autocrine connections (%)
E
Correlation with gap junction network
Correlation with monoaminergic network
Total degree
In-degree
Out-degree
Degree
autocrine connections
AVAL
AVAR
AVBR
AVBL
PVR
URX
PQR
CEP
ADE
PDE
F
DA
VA
DB
VB
DMSR-1
DMSR-7
NPR-5